REDUCED CEMENTITIOUS MATERIAL IN OPTIMIZED CONCRETE MIXTURES: ANNUAL CELL PERFORMANCE REPORT

Contract Number: (C) 1003320 (WO) 3

Task 2A: Annual Cell Performance Report

Principal Investigator
Peter Taylor
Director
National Concrete Pavement Technology Center, Iowa State University

Co-Principal Investigator
Xuhao Wang
Project Manager/Adjunct Assistant Professor
National Concrete Pavement Technology Center, Iowa State University

Performing Organization
National Concrete Pavement Technology Center
Iowa State University
2711 South Loop Drive, Suite 4700
Ames, IA 50010-8664
Phone: 515-294-8103 / Fax: 515-294-0467
www.cptechcenter.org

Sponsored by
Federal Highway Administration
Minnesota Department of Transportation
National Road Research Alliance Transportation Pooled Fund

Lead State Representative
Bernard Izevbekhai
Minnesota Department of Transportation
Office of Materials and Road Research, Mail Stop 645
1400 Gervais Avenue, Maplewood, Minnesota 55109
Phone: 651-366-5454
E-Mail: bernard.izevbekhai@state.mn.us

Table of Contents

LIST OF FIGURES

LIST OF TABLES

ACKNOWLEDGMENTS

The research team would like to express their gratitude to the Minnesota Department of Transportation (MnDOT) for sponsoring this research and the National Road Research Alliance (NRRA) for supporting this work.

INTRODUCTION

This document reports the activities and observations of a research team that performed on-site and laboratory testing of modified concrete mixtures with optimized cementitious materials content placed on two designated field testing cells at the MnROAD facility.

The work explores the performance of test cells cast with optimized concrete mixtures prepared with reduced cementitious materials content. Two concrete paving mixtures with "low" cementitious content, i.e., 500 lb/yd^3, and "lower" cementitious content, i.e., 470 lb/yd^3, were used at two identical (except for concrete mix) cells 138 and 238, respectively. Each cell is about 260 feet long. The primary goal of this work is to monitor the constructability and longevity of the concrete mixtures with reduced cementitious material content. The objectives of this study include:

- Investigate the early-age characteristics (i.e. placement issues, slow strength gain) of concrete paving mixes containing reduced cementitious content
- Assess causes of, or potential for, durability issues with very low cementitious content
- Identify effect of reduced cementitious content on long term serviceability and economics of concrete pavements (i.e. benefits of reduced shrinkage)
- Develop recommended specifications, mixing and placement practices for the use of very low cementitious content concrete paving mixes

PROJECT INFORMATION

The present project investigates the performance of two test cells (138 and 238) constructed with optimized concrete mixtures at MnROAD pavement research facility. Located in Albertville, 40 miles Northwest of Saint Paul Minnesota, the MnROAD research facility consists of two distinct segments of roadway: the Mainline (ML) and the Low Volume Road (LVR). MnROAD was built in 1993, comprising 23 original test cells at the time. As at 2016, there were a total of 69 test cells between the Mainline and LVR. A different pavement type and/or design is used in construction of each of these cells.

The Mainline is a 3.5 mile, 2-lane interstate highway that carries live traffic diverted from Westbound Interstate 94 while the LVR is a 2-lane wide closed loop with 24 test cells (in 2016) with a total length of 2.5 miles. The traffic on the LVR is restricted to a single 18-wheel, 5-axle tractor with trailer that is intended to simulate the traffic conditions on rural roads. Operation of this vehicle is performed by the MnROAD staff and according to a controlled schedule that includes 80 laps per day on the inside lane only. The outside lane is subjected to environmental loading only, except for the minimal loading from lightweight test vehicles. This restriction is intended to demonstrate the pavement response due to environmental effects versus loading effects.

The low cementitious test cells 138 and 238 are contiguously located on the LVR as presented in Figure 1. A concrete mixture with 500 lb/yd^3 of cementitious materials was used for building Cell 138 and designated as the low cementitious mixture, while another similar mixture proportioned with 470 lb/yd^3 of cementitious materials content was used for Cell 238 and designated as the lower cementitious mixture in this report. Data obtained from these two cells were compared to those gathered from testing the Cell 524 proportioned with 570 lb/yd^3 of cementitious materials that serves as the reference Cell in this study.

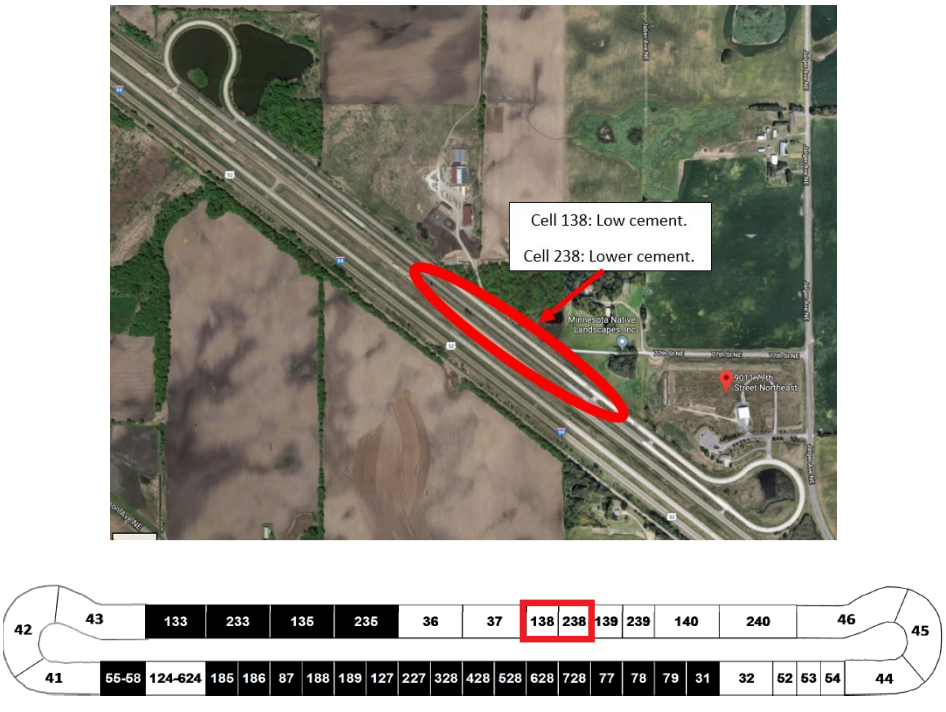

Figure 1- Aerial photo (top) and schematic view (bot.) of the investigated cells

Concrete placement, sampling, and testing took place on July 14, 2017. The construction activities, design details, and research activities of each test cell were identical:

- Construction activities
  - Remove 258 feet of existing concrete pavement
  - Repair existing Class 5 base (if damaged)
  - Install sensors, including vibrating wire strain gauges, quarter-bridge strain gauges, thermocouple trees and maturity loggers (shown in Table 1)
  - Install T2 plates (for thickness verification)
  - Place new concrete layer and conduct tests during paving (shown in Table 2 and Table 3)
  - Fabricate research samples (cylinders/beams) for further lab testing (shown in Table 4)
  - Place new gravel shoulders
- Design details (shown in Figure 2)
  - Panel thickness = 8 inches
  - Panel size = 12 ft W x 15 ft L driving lane
  - Low cementitious mixture with 500 lb/yd^3 of cementitious materials at Cell 138 and lower cementitious mixture with 470 lb/yd^3 of cementitious materials at Cell 238
  - Shoulders = 2 inch thick shoulder gravel
  - Dowel bars = 1.25 inch diameter epoxy coated steel in standard MnDOT pattern
  - Joints = Single 0.125 inch width saw cut, depth = T/4, unsealed
  - Base: 5.0 in. Class 5 aggregate base
  - Subgrade: Clay loam (A-6)

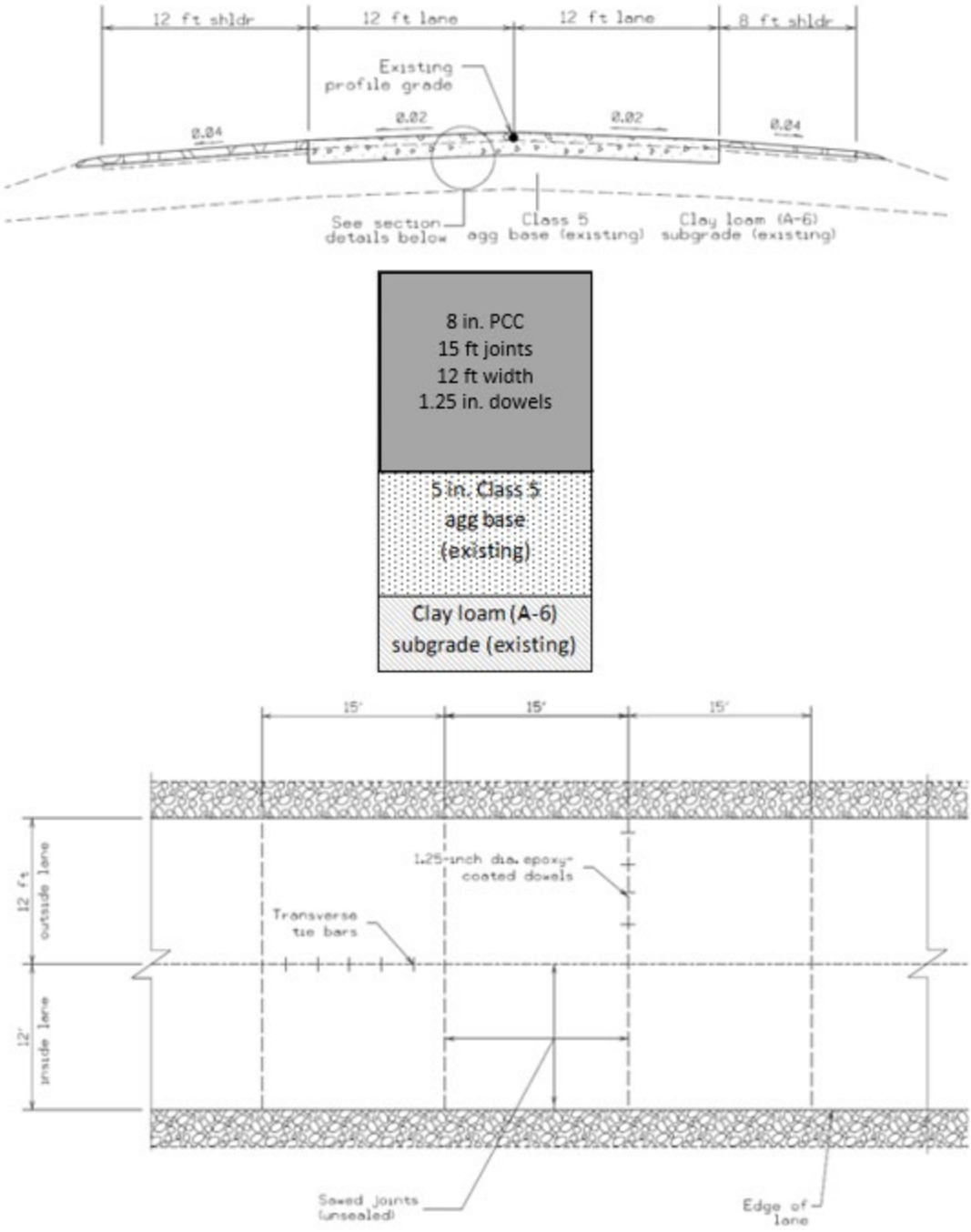

Figure 2- Pavement construction details

Research activities shown in Tables 1-4 include early and long-term research activities; tests during paving and lab testing using fabricated research samples.

Table 1- Pre-paving activities

Pre-Paving				
Project Test Matrix	**Test Ages**	**Number of Sensors**	**Cure Procedure**	**Conducted by**
Vibrating Wire Strain Gauges	On-site sensor installation /Continuous	4	In the pavement	MnDOT
Quarter-bridge Strain Gauges		8		
Thermocouple Trees		2		
Maturity Logger		1		
5TE Moisture Sensor		2		

Table 2- Research activities during paving

During Paving					
Project Test Matrix	**Test Age**	**Type of Test Specimens**	**Size of Specimens**	**Number of Specimens**	**Conducted by**
AASHTO PP84, Box Test	Fresh	Cube	9.5 in3	1	MnDOT
AASHTO TP129, VKelly Test	Fresh	Tub	17x15x8 -inch rubber tub	3	ISU
AASHTO PP84, SAM Test	Fresh	Air pot	0.25 cf	1	MnDOT/ISU
AdiaCal Calorimetry: semi-adiabatic measurement on concrete temperature	up to 1 day	Cylinders	4x8-inch	2	ISU
AASHTO T318, Microwave w/cm ratio	Fresh	Bowl	~2,000 g	1	ISU
ASTM C138, Unit Weight	Fresh	Air pot	0.25 cf	1	MnDOT/ISU

Table 3- Early research activities

Early Research Activities		
Test	**Location**	**Conducted by**
Monitor maturity	Paving cell/ In the pavement	MnDOT
Conduct early-age warp and curl tests		MnDOT
Monitor joint deployment using MIRA		ISU
Baseline FWD and truck load tests		MnDOT

Table 4- Hardened concrete testing plan for laboratory

Post-Testing							
Project Test Matrix	**Test Age (day)**	**Type of Test Specimens**	**Specimen Size**	**Number of Specimens**	**Curing**	**Cure Time**	**Conducted by**
ASTM C39, Compressive Strength	2 , 3 , 7 and 28 days	Cylinders	6x12-inch 2 per test	8	Moist Room	Per test age	MnDOT
ASTM C78, Flexural Strength	2 , 3 , 7 and 28 days	Beams	6x6x20-inch 1 per test	4	Lime-water	Per test age	MnDOT
ASTM C666, Proc. A Freezing and Thawing in Water	14 days	Cores	3x3x11¼-inch, set of three beams	3 beams	Lime-water	14 days	MnDOT
AASHTO T336, Coefficient of Thermal Expansion	28 days	Cylinder	4x8-inch	1	Moist Room	28 days	MnDOT
ASTM C469, Modulus of Elasticity and Poisson's	28 days	Cylinder	6x12-inch	1	Per test method	28 days	MnDOT
ASTM C215, Dynamic Modulus	7 and 28 days	Cylinder	4x8-inch	1	Moist Room	28 days	MnDOT
Wenner Probe Resistivity	28 days	Cylinder	4x8-inch	2	Per test method	28 days	MnDOT/ISU
ASTM C856, Brief Petrographic Examination of Hardened Concrete: estimated air content; degraded air system; microcracking	After ASTM C666 testing	Tested freeze-thaw beam	3x3x11¼ inch	1	Lime-water	14 days	MnDOT
ASTM C457, Air Void Analysis of Hardened Concrete	at least 14 days	Tested freeze-thaw beam	4x8-inch cylinder	1	At least 14 days moist cure	14 days moist cure	MnDOT
ASTM C157, Drying Shrinkage	56 days	Beams	4x4x11¼-in beams with pins	1	28 days lime-water	28 days	MnDOT
AASHTO PP84, Bucket Test	14 days up to 90 days	Cylinders	4x8-inch	3	lime-water	60 days	ISU
Modified ASTM C29, Dry Rodded Unit Weight and Voids in Combined Aggregate Systems	-	Aggregates	80 lbs	3	-	-	ISU
AASHTO PP84, Low Temperature Differential Scanning Calorimetry (LT-DSC)	after 28 days	Cylinder	4x8-inch	1	50C sealed oven cure	28 days	ISU

MATERIALS

Cementitious Materials

Type I/II Portland cement (ASTM C150) and Class F fly ash (ASTM C618) were used as the cementitious mixtures for all mixtures. A binary system with 25% (by mass) fly ash replacement was designed.

Aggregate

A single source of coarse aggregate, two types of intermediate aggregates, and a natural river sand were used. Table 5 summarizes the physical properties of aggregates.

Table 5- Aggregate properties

Aggregate Type	Specific Gravity (SSD)	Water Absorption (%)
Coarse	2.73	0.90
Intermediate #1	2.69	1.30
Intermediate #2	2.67	1.50
River Sand	2.63	0.90

Both concrete mixtures were proportioned with an optimized aggregate system, with a weight fraction of 18% coarse aggregate, 33% intermediate #1, 10% intermediate #2, and 39% fine aggregate. The combined aggregate gradations were plotted in a Tarantula curve (Ley et al. 2012), power 45 curve (Kennedy et al. 1994), and Shilstone workability factor chart (Shilstone 1990), as shown in Figure 3.

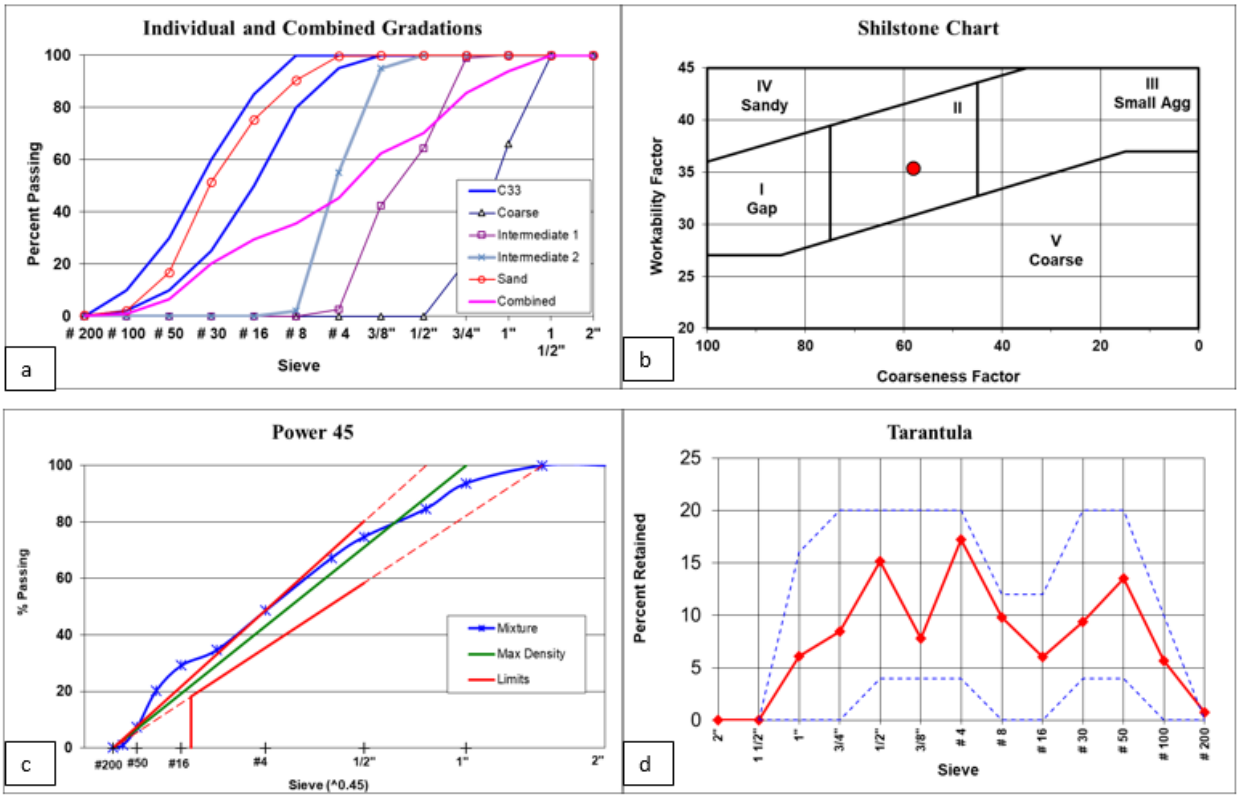

Figure 3- (a) Individual and combined gradations, (b) workability factor chart, (c) power 45 chart, and (d) Tarantula curve

In the workability factor chart, the workability and coarseness factors of the aggregate system fall within Zone II. The combined aggregate system also met the recommendations of the Tarantula plot.

Mixture Proportions

Table 6 offers a summary of the mixture proportions used for casting the pavement at Cells 138 and 238, as well as the concrete mixture used for casting the reference pavement at Cell 524. The mixtures used for building Cells 138 and 238 were proportioned with fixed w/cm of 0.42, while a w/cm of 0.40 was used for the reference concrete used in construction of Cell 524. A binary cement with 25% Class F replacement was used for mixtures with Low and Lower cementitious materials content, compared to 30% fly ash replacement in reference mixture. Air entraining admixture (AEA) and high range water reducing admixture (HRWRA) were used to secure required fresh properties. The percentage voids in aggregate was 27.3% determined based on modified ASTM C 29. Results were incorporated in determining the paste to combined aggregate voids volume ratio (V_{paste}/V_{voids}) using the approach described by Taylor et al. (2015). This approach suggests that V_{paste}/V_{voids} should range between 125 and 175 percent.

Table 6- Concrete mixture proportions

Mix ID	**Unit**	**Type**	**Low Cementitious (Cell 138)**	**Lower Cementitious (Cell 238)**	**Reference (Cell 524)**
Cement	lb/yd^3	Type I/II	375	353	400
Fly Ash	lb/yd^3	Class F	125	117	170
Water	lb/yd^3		210	197	228
w/cm			0.42	0.42	0.40
Coarse Agg.	lb/yd^3		322	328	562
Intermediate #1	lb/yd^3		1,071	1,091	1,015
Intermediate #2	lb/yd^3		589	600	305
Fine Agg.	lb/yd^3		1,235	1,258	1,173
Air Entraining Admixture	oz/cwt		1.0	2.0	
Water Reducing Admixture	oz/cwt	High Range	1.0	1.0	
SCM Dosage	% mass		25	25	30
V_{paste}/V_{voids}	%		146	137	
Unit Weight	lb/ft^3		145.4	146.1	

TEST METHODS

The test program considered for investigating the properties of incorporated concrete mixtures and performance of the investigated cells can be divided into three stages:

- Field tests aimed at assessing the robustness and consistency of the concrete mixtures used for building the cells
- Use of instrumentation and in-situ tests aimed at exploring the performance of the pavements over time.
- Laboratory tests aimed at investigating the strength development, durability in terms of transport properties, and joint deterioration potential of the concrete mixtures used for building the cells. Samples for lab tests were fabricated in the field.

The following field tests were conducted:

- VKelly (AASHTO TP 129) (Figure 4)
- Box test (Cook et al. 2014) (Figure 5)
- Super air meter (SAM) (Ley 2013)
- Air content (ASTM C 231 2014)
- Unit weight (ASTM C 29 2009)
- Microwave water/cementitious ratio
- Semi-adiabatic calorimetry (ASTM C 1753 2015) (Figure 6)
- Maturity, using embedded sensors

The following laboratory tests were conducted:

- Compressive strength measurement (ASTM C 39)
- Modulus of elasticity and Poisson's ratio (ASTM C 469)
- Flexural strength (ASTM C 78)
- Air-void system in hardened state (ASTM C 457)
- Coefficient of thermal expansion (AASHTO T 336)
- Drying shrinkage (ASTM C 157)
- Surface resistivity (AASHTO TP 95 2011) up to 91 days (cylinders)
- Formation factor (AASHTO PP 84-17) up to 91 days (cylinders)
- Low-temperature differential scanning calorimetry

The following instrumentations and in-situ tests were conducted:

- Falling weight deflectometer (MnDOT's FWD Tester, ASTM E2583 07-2015)
- Ride quality (MnDOT's Light Weight Profiler, ASTM E-950)
- Dynamic load test (MnROAD Semi Tractor Trailer)
- Deformations due to environmental conditions (Vibrating Wire Strain Gages)
- Evaluating the joint activation using MIRA
- Distress survey (In-situ inspection)

Figure 4- VKelly test setup

Figure 5- Box test showing voids on concrete surface

Figure 6- Calorimetry test setup for measuring the heat of hydration

RESULTS

This section summarizes the data collected during the first year from construction of the investigated cells. Specific tests are discussed below.

Ambient Conditions

The ambient temperature during field testing were in the range of 61.3 to 68.0°F, relative humidity varied from 67 to 87 percent, and wind speed was 3.0 mph.

Field Tests

VKelly Test

The VKelly tests indicated that the slump of the mixtures used for Cells 138 and 238 were 2.50 and 1.50 in., respectively. The VKelly index of 0.50 in./$s^{0.5}$ obtained for mixture with lower cementitious content was slightly lower than the recommended minimum of 0.60 in./$S^{0.5}$. However, the mixture with low cementitious content used for Cell 138 exhibited a VKelly index of 0.88 in./$s^{0.5}$, which was within the recommended range (Taylor et al. 2015). Slight adjustments in WRA dosage were necessary to achieve desirable workability during paving with concrete containing lower cementitious materials content.

Box Test

The box test indicated better workability for mixture with low cementitious content. An average visual rating of 1.0 was reported for this mixture, corresponding to less than 10 percent overall surface voids. The visual rating was between 2 and 3 for the concrete with lower cementitious content, indicating 30-50 percent overall surface voids (Cook et al. 2014). No edge slump was observed for the mixtures.

Super Air Meter (SAM) Test

The SAM test was conducted to measure the air content in fresh state, as well as the quality of the air void system. Two measurements were performed for each concrete type. The average air content in fresh state was 8.5% and 6.5% for the mixtures with “low” and “lower” cementitious materials contents, respectively, with average SAM numbers of 0.26 and 0.22. Ley (2013) recommends a SAM value below 0.2, which is associated with a spacing factor below 0.008 in for acceptable freeze-thaw durability. The fresh air-void system data obtained for the mixtures used in construction of Cells 138 and 238 suggest proper durability against freeze and thaw cycles.

Unit Weight

The average unit weight was 143.0 and 148.1 lb/ft^3 for the mixtures with “low” and “lower” cementitious materials contents, respectively. The theoretical unit weight was 145.4 and 146.1 lb/ft^3 for these mixtures, respectively.

Microwave Water Content

The microwave test indicated average w/cm of 0.41 and 0.44 for the mixtures prepared with low and lower contents of cementitious materials, respectively. It is worth mentioning that the design w/cm was 0.42 for both mixtures. The higher w/cm of 0.44 obtained for concrete used in building the Cell 238 can raise concerns regarding the long-term durability of this cell. Increase in shrinkage and lower transport properties could be expected for this mixture.

Semi-Adiabatic Calorimetry

The calorimetry curves are presented in Figure 7, and temperature rise data are plotted in Figure 8. No significant difference in temperature rise was observed for the first 10 hours, while slightly higher values were observed for the concrete proportioned with low cementitious materials content afterwards.

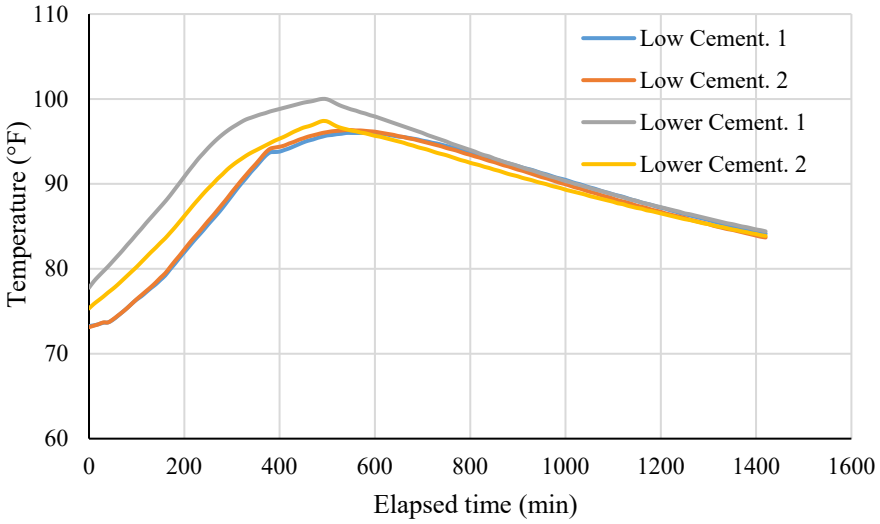

Figure 7- Semi-adiabatic calorimetry results

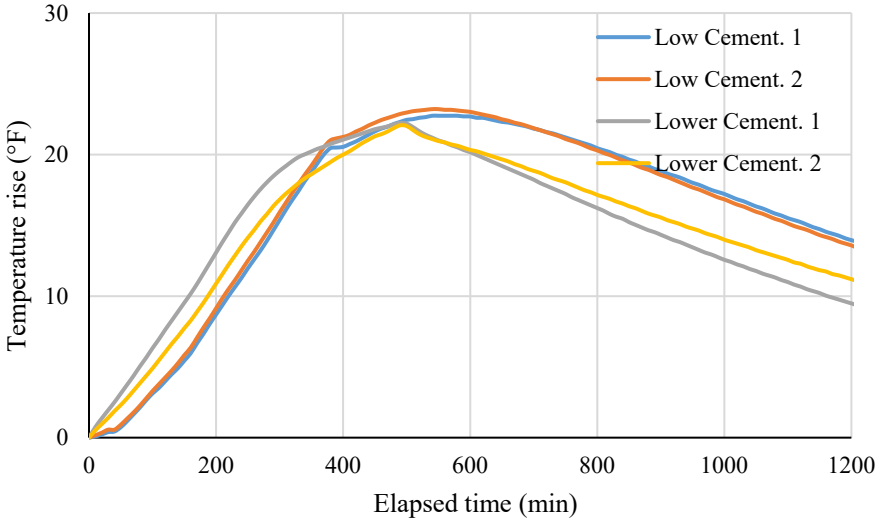

Figure 8- Semi-adiabatic calorimetry temperature rise

The minor variations in temperature raise for the investigated mixtures presented in Figure 8 is believed to be due to the lower cementitious materials content used in construction of Cell 238. However, no abnormalities were observed in terms of delayed setting time or strength development of either of the mixtures and no issues were observed later on during saw cutting the joints.

Maturity

Figure 9 presents the average maturity data recorded for the mixtures. Similar performance was observed, regardless of the binder content. This was expected given the same binder composition used in both mixtures. Observations were in agreement with the calorimetry results and early age compressive strength data obtained through laboratory testing (discussed in following sections).

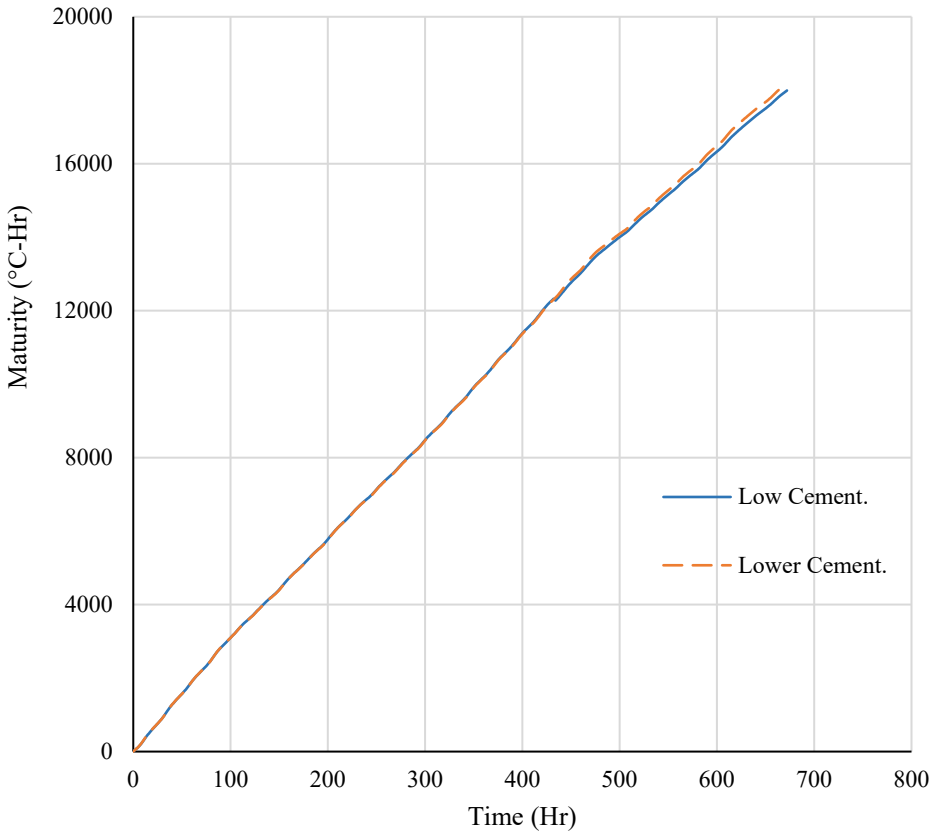

Figure 9- Average maturity data

Hardened Concrete Properties – Laboratory Measurements

Compressive Strength

The average compressive strength of the mixtures is presented in Figure 10 for up to 28 days. Both mixtures developed comparable compressive strength regardless of the binder content. Both mixtures exhibited a 48-hour strength of approximately 1,750 psi and 28-day strength of higher than 3,500 psi as required by AASHTO PP 84. Both mixtures exhibited the compressive strength of 3,000 psi, required for opening to traffic (MnDOT2016), before 14 days. The slightly higher 28-day compressive strength of the concrete with lower cementitious materials content may be attributed to the lower air content observed for this concrete (6.5% vs. 8.5%).

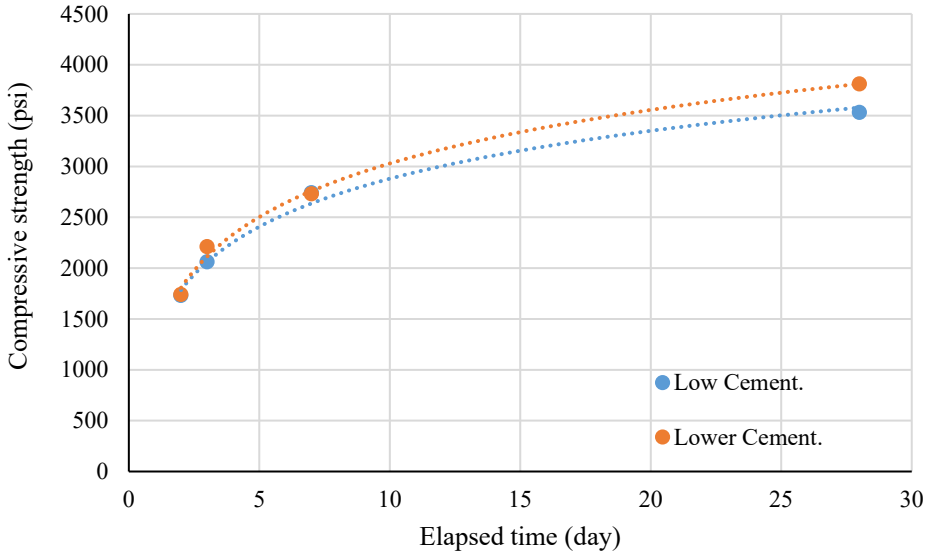

Figure 10- Compressive strength results

Modulus of Elasticity and Poisson's Ratio

Static modulus of elasticity (MOE) and Poisson's ratio measurements were conducted at 28 days. The mixture prepared with lower binder content exhibited 28-day MOE of 5.43×10^6 psi, in comparison to 5.26×10^6 psi, for the concrete with low cementitious materials. This can be due to the slightly higher aggregate content in concrete prepared with lower binder content. The 28-day Poisson's ratio values were 0.21 and 0.17 for the mixtures made with lower and low cementitious materials content, respectively. Assuming similar base conditions, and considering the same thickness of the pavements, comparable MOE values obtained for the two mixtures suggest similar response to traffic loading for the investigated cells.

Flexural Strength

Flexural strength measurements were conducted at 3, 7, and 28 days. Results are presented in Figure 11. The mixture prepared with low cementitious materials content exhibited a linear trend in flexural strength development, with a 28-day value of 615 psi. The concrete with lower cementitious materials content developed a relatively low 3-day flexural strength of 170 psi. However, the 7- and 28-day flexural strength values for this mixture were comparable to those of the concrete with low cementitious materials

content. The 7- and 28-day flexural strength values for concrete made with lower cementitious materials content were 475 and 625 psi, respectively.

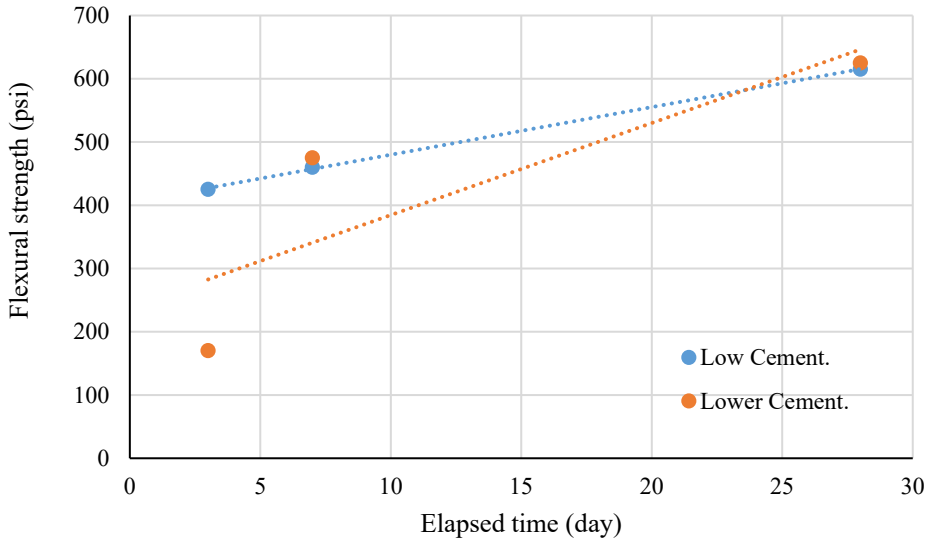

Figure 11- Flexural strength measurements

In general, it was observed that the mixtures prepared with Low and Lower cementitious materials content, used for building the cells 138 and 238, respectively, exhibited comparable mechanical properties. This is in line with the comparable in-situ performance data obtained from testing the Cells 138 and 238.

Hardened Air-Void Analysis

An approximate reduction of 1.0% in air content of hardened samples was observed in comparison with the results in the fresh state. Analysis of the hardened specimens indicated an air content of 7.5% for the concrete with low cementitious content (Cell 138) and air content of 5.3% for mixture made with lower binder content (Cell 238). Both these mixtures exhibited spacing factor of 0.002 in. and specific surface area within the range of 1500±100 $in.^2/in.^3$. A spacing factor of no more than 0.008 in. is generally recommended in order to secure a desirable air-void system in moderate exposures (ASTM C 457). The air-void system data obtained in fresh and hardened states suggests potential for desired durability against freezing and thawing cycles. Data obtained during the first year certifies the acceptable performance of the investigated cells. The research team will continue monitoring the cells for signs of any freeze-thaw related distress for the next two years.

Coefficient of Thermal Expansion (CTE)

CTE measurement was conducted at 28 days. Both mixtures exhibited a CTE of 5.0×10^{-6} in./in./°F. Lower CTE values can reduce the thermal deformation of rigid pavements. The obtained values were reasonably low compared to the typical values expected for pavement concrete. These were in line with the comparable response of the pavement sections to environmental effects, where both cells exhibited similar strain values and deformation patterns (discussed in following sections).

Drying Shrinkage

Shrinkage measurements were conducted at 56 days, including 28 days of moist curing followed by 28 days of drying. The concrete with low cementitious content exhibited a slightly lower shrinkage of 370 με compared to 410 με for the mixture with lower binder content. Even though both numbers can be considered as adequately low drying shrinkage values, this observation can be attributed to the slightly higher w/cm measured for the concrete with lower cementitious content determined through micro wave test (w/cm of 0.44 vs. 0.41).

Surface Resistivity Test

The criteria for assessing surface resistivity, as proposed by AASHTO PP 84, are summarized in Table 7. The average surface resistivity measurements are presented in Figure 12. The investigated mixtures exhibited comparable resistivity, with 91-day values of about 25.0 kohm-cm, corresponding to "Very Low" risk of chloride ion penetration at 91 days. The increasing surface resistivity over time indicates potentially improved performance in the long-term.

Table 7- Chloride ion penetrability classification (Adapted from AASHTO PP 84)

Chloride Ion Penetrability	**Greatest Resistivity (kohm-cm)**	**Lowest Resistivity (kohm-cm)**
High	5	~
Moderate	10	5
Low	20	10
Very Low	200	20
Negligible	~	200

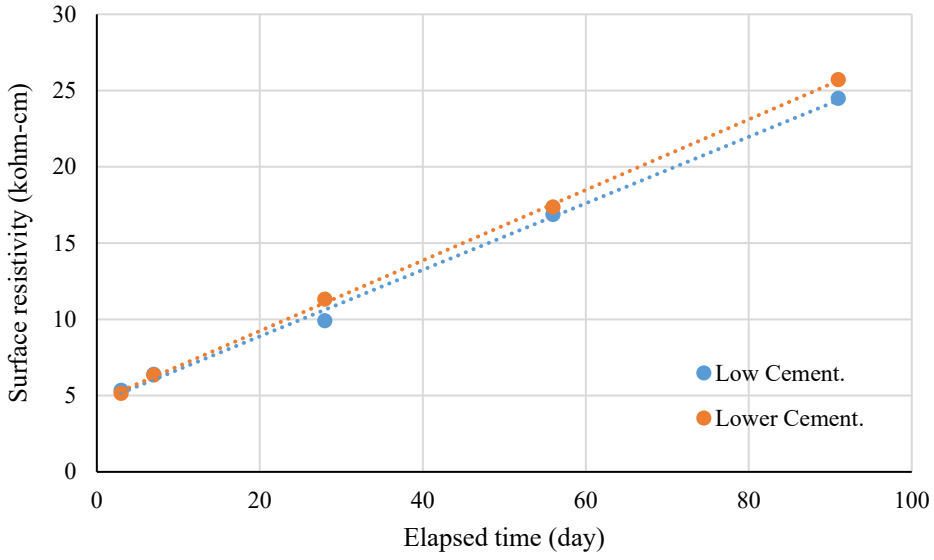

Figure 12- Surface resistivity measurements

Formation Factor

Formation factor (FF) development is presented in Figure 13. Measurements are based on assuming a pore solution resistivity of 0.10 Kohm-cm as suggested by Barrett et al. (2016). Reported data are based on moist cured samples rather than vacuum saturated specimens. The investigated mixtures exhibited similar FF values, with 91-day measurements of about 2500, corresponding to "Very Low" chloride ion penetrability as proposed by AASHTO PP 84 (2017).

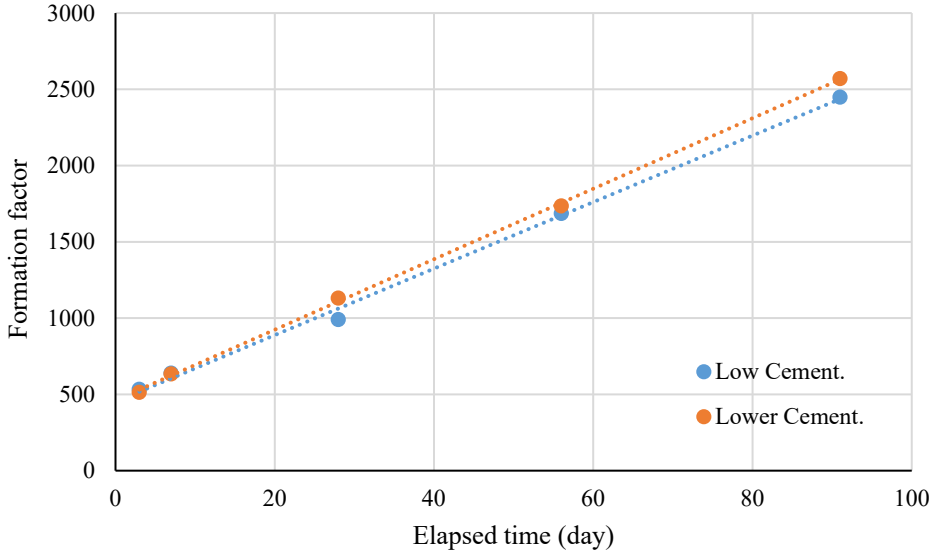

Figure 13- Formation factor results

Low-Temperature Differential Scanning Calorimetry

Monical et al. (2016) have proposed a method using low-temperature differential scanning calorimetry (LT-DSC) to quantify the potential for calcium oxychloride formation for cementitious materials in the presence of calcium chloride.

Samples from both mixtures were prepared by grinding hardened paste to a powder that passed through a 75-µm sieve (No. 200). A calcium chloride solution was prepared at a concentration of 20 percent $CaCl_2$ by mass. Then, 10 ±1 mg of powder specimen was mixed with the solution in a powder-to-solution mass ratio of 1 to 1 and tested in accordance with the following procedure (Monical et al. 2016):

1. Store the sample at room temperature for approximately 1 hour after combining the cementitious powder and salt solution to permit any heat associated with the hydration of exposed unreacted surfaces of cementitious materials to dissipate

2. Reduce the temperature to -90˚C at a rate of 3˚C/min and start logging data

3. After reaching -90˚C, expose the sample to a low-temperature loop (cycling the temperature from -90˚C to -70˚C back to -90˚C at a rate of ±3˚C/min) until the solution has frozen

4. Heat the sample at a rate of 0.25˚C/min until the sample reaches a temperature of 50˚C; then, allow the sample to return to room temperature

The heat absorbed during the calcium oxychloride melting phase is evaluated by integrating the heat flow versus time curve. The energy associated with the calcium oxychloride formation can be estimated by measuring the magnitude of the shift in cumulative heat slopes before and after the phase transformation (i.e., the drop in the cumulative heat curve between points A and C, as shown in Figure 14).

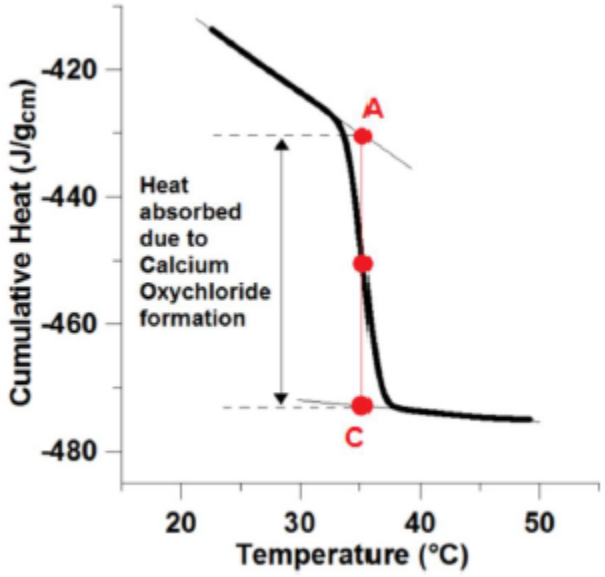

Figure 14- The drop associated with calcium oxychloride formation in cumulative heat curve (Monical et al. 2016)

The specific latent heat can be used to quantify the amount calcium oxychloride through Equation 3:

$$m_{oxy} = \frac{\Delta H_{oxy}}{L_{oxy}} \tag{3}$$

Where, m_{oxy} is the gram of calcium oxychloride per gram of cementitious binder, ΔH_{oxy} (joule per gram of cementitious material) is the latent heat absorbed during the calcium oxychloride phase transformation calculated for samples with different cementitious materials, and L_{oxy} (joule per gram of oxychloride) is the specific latent heat associated with calcium oxychloride phase transformation, which is 186 J/g.

The cumulative heat flow based on LT-DSC results was 6.36 for both investigated mixtures. A typical DSC curve is presented in Figure 15. This resulted in 0.186 and 0.205 gram of calcium oxychloride per gram of paste for the mixtures with low and lower cementitious materials content, respectively. A value of less than 0.15 gram of calcium oxychloride per gram of paste is recommended by AASHTO PP 84 to ensure low risk of oxychloride formation. This indicates that the investigated cells (138 and 238) can be prone to the risk of oxychloride formation if subjected to de-icing salts.

One should note that the electrical resistivity measurement is a function of system porosity and transport properties. However, the oxychloride formation risk is a function of binder chemistry. Therefore, the observations from these two test will not necessarily follow the same trend.

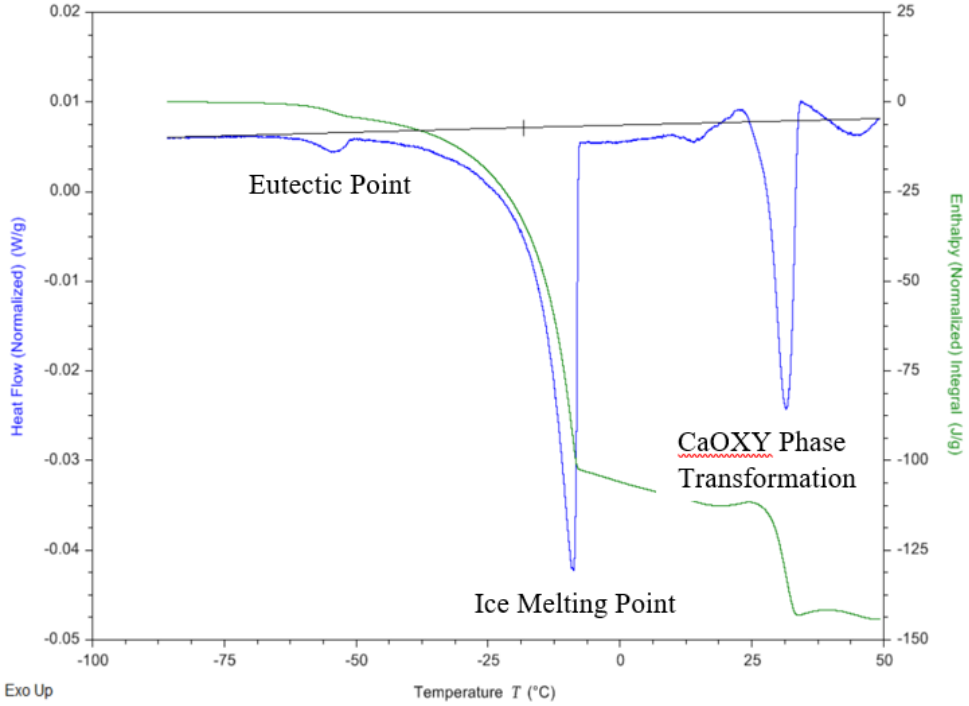

Figure 15- A typical LT-DSC curve

Pavement Performance – In-Situ Measurements

Falling Weight Deflectometer

Falling weight deflectometer (FWD) test was conducted on pavement cast with reduced cement content and reference mixture according to the following matrix. Note that the reference cell (Cell 524) is 6.0 in. thick, while the 138 and 238 Cells were 8.0 in. thick. MnDOT's FWD tester, conforming to requirements of the ASTM E2583 was used for testing the cells. The test setup is shown in Figure 16 .

Figure 16- MnDOT's FWD tester

Test dates:

Reference pavement (Cell 524): 09/14/2017, 10/23/2017, 03/15/2018

Pavement with low (Cell 138) and lower cementitious materials (Cell 238): 09/06/2017, 10/24/2017, 03/27/2018, and 05/03/2018

Investigated lanes:

Inside lane and outside lane for all concrete types

Investigated slabs:

Reference pavement (Cell 524): slab #0 and #2

Low cement pavement (Cell 138): slab #4, #7, #11, and #14

Lower cement pavement (Cell 238): slab #2, #6, #9, and #13

Test positions:

Slab center, corner, mid-edge, joint before, and joint after for all concrete types

Load amounts:

Deflections were collected for one drop at each load level of 6000, 9000, and 12000 lbs, corresponding to approximate stress level of 390, 570, and 750 KPa.

Sensor offsets:

Ten sensors were incorporated to collect the deformation at various distances with respect to the center of the load plate. Table 8 summarizes the sensor spacing.

Table 8- FWD sensor spacing from center of the load plate

Sensor #	1	2	3	4	5	6	7	8	9	10
Distance (in.)	0	8	12	18	24	36	48	60	72	-12

Test data obtained from FWD testing conducted before and after the transverse joints, corresponding to approaching and departure traffics, respectively, were used to calculate the load transfer efficiency (LTE) according to Equation 1.

$$LTE = \frac{\delta_U}{\delta_L} \times 100\% \quad (1)$$

where δ_U is the deflection of the unloaded side of the joint (mm), δ_L is the deflection of the loaded side of the joint (mm), and LTE is the load transfer efficiency (%).

Results are summarized in Tables 9 to 11 for the pavement cast with low cement, lower cement, and reference concrete mixtures, respectively. The values reported in these tables summarize the data obtained for both inside and outside lanes exposed to approaching and departure traffic, also known as “Before Joint” and “After Joint” measurements, respectively.

Results obtained for inside lane of Cell 138 cast with low cementitious materials content indicated LTE values ranging from 79% to 96%, and from 80% to 95% for the approach and departure traffics, respectively. LTE values obtained for the outside lane ranged from 82% to 93% and from 83% to 97% for the approach and departure traffics, respectively.

Similar data were obtained from Cell 238, indicating comparable LTE for the departure and approaching traffics for both lanes. For the inside lane, the LTE ranged from 78% to 95% for the approaching and from 82% to 97% for the departure traffic, respectively. LTE results were between 85% and 94% for the outside lanes, regardless of the traffic direction.

Slight reduction in LTE was observed for the reference pavement with average data between 84% and 86%. This can be due to the lower thickness of the reference cell compared to the low cement sections.

The LTE data are summarized in Figure 17. In general a linear correlation was observed for the LTE values obtained for the approaching and the departure traffic. In general the LTE values obtained for Cells 138 and 238 were comparable, indicating similar load transfer characteristics for these two cells. For both cells, the comparison between the LTE values for departure and approaching traffic indicated higher scatter in LTE values for the inside lane exposed to regular traffic loading. In summary, the LTE values obtained for Cells 138 and 238 suggested similar performance during the first year.

Table 9- Average LTE data obtained for concrete with low cement content (Cell 138)

Test Date	Slab ID	Approach Traffic		Departure Traffic	
		Inside	Outside	Inside	Outside
09/06/2017	4	86.7	90.6	86.0	94.4
	7	87.2	90.2	89.5	90.7
	11	89.5	92.4	94.8	97.1
	14	87.8	91.0	89.2	89.5
10/24/2017	4	91.7	92.4	90.5	92.7
	7	90.4	91.4	88.6	90.6
	11	96.0	93.0	92.5	92.1
	14	92.6	88.4	87.8	93.1
03/27/2018	4	79.1	87.2	83.2	87.6
	7	86.4	83.8	80.5	83.7
	11	90.0	81.6	87.0	82.8
	14	89.0	82.7	84.9	84.6
Average	4	85.8	90.1	86.6	91.6
	7	88.0	88.5	86.2	88.3
	11	91.8	89.0	91.4	90.7
	14	89.8	87.4	87.3	89.1

Table 10- Average LTE data obtained for concrete with lower cement content (Cell 238)

Test Date	Slab ID	Approach Traffic		Departure Traffic	
		Inside	Outside	Inside	Outside
09/06/2017	2	-	91.0	-	90.9
	6	92.8	88.3	96.7	90.0
	9	94.7	89.2	91.2	91.8
	13	86.9	90.9	95.7	89.9
10/24/2017	2	90.5	92.4	89.1	93.5
	6	90.7	91.4	89.8	91.3
	9	91.4	91.7	89.4	90.5
	13	91.0	94.1	89.2	92.9
03/27/2018	2	78.2	86.4	83.0	86.9
	6	88.7	85.1	85.7	83.6
	9	85.4	84.7	82.7	83.9
	13	83.0	87.2	82.3	84.2
Average	2	84.4	89.9	86.1	90.4
	6	90.7	88.3	90.7	88.3
	9	90.5	88.5	87.8	88.7
	13	87.0	90.7	89.1	89.0

Table 11- Average LTE data obtained for reference concrete (Cell 524)

Test Date	Slab ID	Approach Traffic		Departure Traffic	
		Inside	Outside	Inside	Outside
10/23/2017	2	92.9	89.0	91.4	84.5
	0	90.4	87.9	92.1	89.1
03/15/2018	2	87.1	75.0	87.7	77.4
	0	77.9	77.7	75.7	80.9
Average	2	90.0	82.0	89.6	81.0
	0	84.2	82.8	83.9	85.0

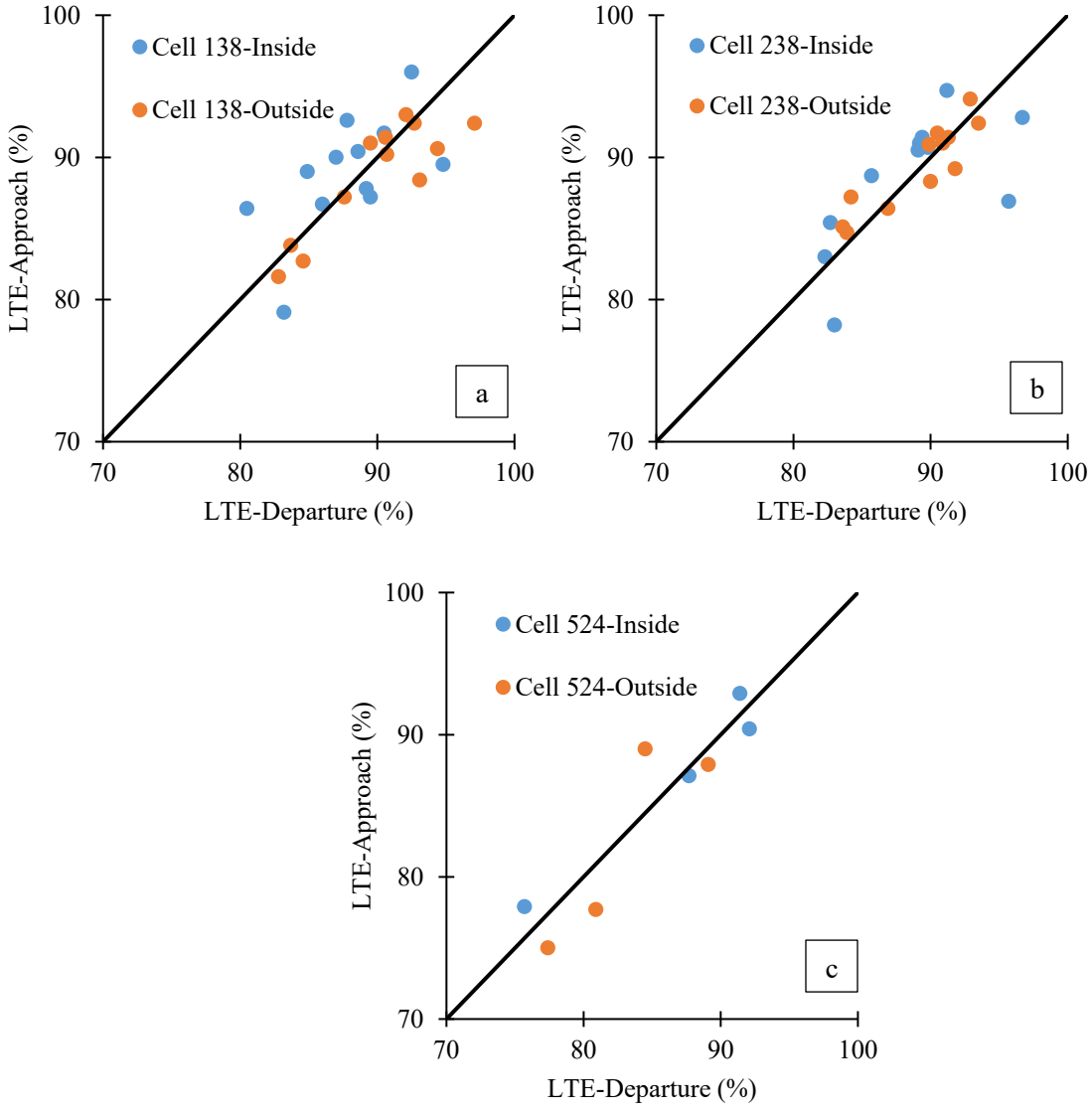

Figure 17- Variation in LTE as a function of traffic direction for low cement concrete (a), concrete with lower cementitious content (b), and reference mixture (c)

Data obtained from testing the slab at interior positions were employed for determining the modulus of subgrade reaction (K) values for the investigated panels according to AASHTO (1993). The area of deflection basin corresponding to 9000 lb loading was initially calculated based on Equation 2 (AASHTO 1993):

$$AREA = 6 \times \left[1 + 2\left(\frac{\delta_{12}}{\delta_0}\right) + 2\left(\frac{\delta_{24}}{\delta_0}\right) + \left(\frac{\delta_{36}}{\delta_0}\right)\right] \quad (2)$$

where δ_0 is the deflection in the center of loading plate (mm), δ_{12} is the deflection at 12 inches from the plate center (mm), δ_{24} is the deflection at 24 inches from the plate center (mm), and δ_{36} is the deflection at 36 inches from the plate center (mm).

Figure 18 proposed by AASHTO (1993) was then used for calculation of the dynamic K-value based on the calculated AREA and deflection at the center of the loading plate (mils).

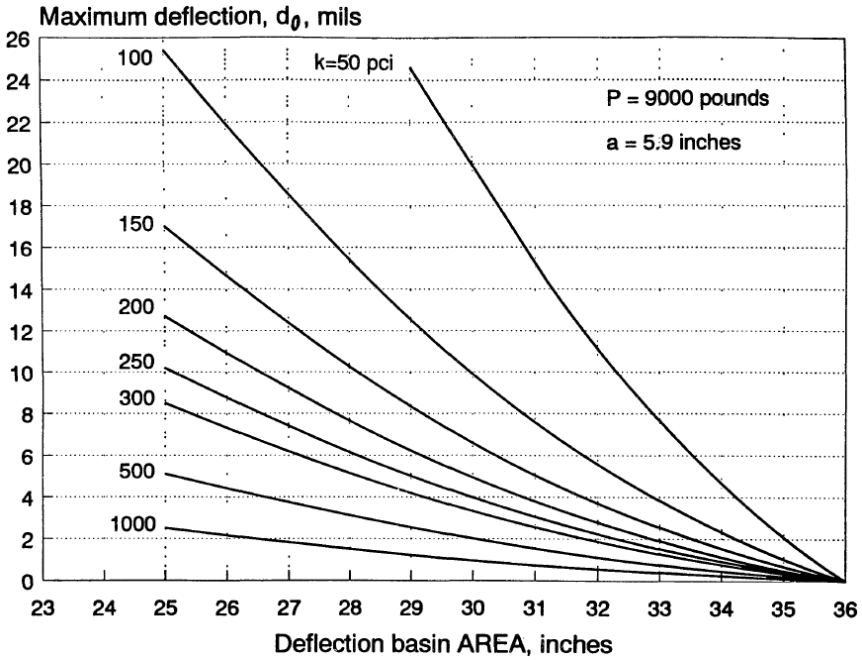

Figure 18- Dynamic k-value as a function of AREA and deflection at the center of the loading plate, borrowed from AASHTO (1993)

Table 12 summarizes the dynamic k-values obtained for the investigated slabs at different testing times obtained for center, corner, and mid-edge of the slabs at inside and outside lanes. The values reported in this table will serve as reference for over-time monitoring the subgrade performance.

In general the k-values were higher for the pavement cast with the reference concrete, indicating better preparation of the subgrade materials. It should be noted that the Cell 524 has a sand subgrade versus a clay/loam subgrade for Cells 138 and 238. Moreover, test results obtained for the reference cell (Cell 524) are affected by the lower slab thickness of 6.0 in. compared to 8.0 in. for Cells 138 and 238.

Table 12- Average dynamic k-values (psi)

Cell	Spot	Slab	Test Date						
			09/06/17	09/14/17	10/23/17	10/24/17	03/15/18	03/27/18	05/03/18
138	Center	4	200	-	-	180	-	350	148
		7	168	-	-	195	-	363	150
		11	178	-	-	163	-	235	175
		14	160	-	-	150	-	285	148
238		2	165	-	-	163	-	270	153
		6	180	-	-	183	-	370	158
		9	168	-	-	175	-	243	158
		13	148	-	-	135	-	265	140
524		0	-	378	250	-	253	-	-
		2	-	315	233	-	250	-	-
138	Corner	4	143	-	-	163	-	155	-
		7	155	-	-	138	-	150	-
		11	135	-	-	130	-	158	-
		14	143	-	-	138	-	150	-
238		2	138	-	-	166	-	160	-
		6	140	-	-	138	-	150	-
		9	130	-	-	145	-	160	-
		13	140	-	-	158	-	153	-
524		0	-	-	-	-	230	-	-
		2	-	-	-	-	205	-	-
138	Mid-edge	4	100	-	-	83	-	130	-
		7	80	-	-	83	-	105	-
		11	113	-	-	88	-	108	-
		14	93	-	-	83	-	123	-
238		2	80	-	-	98	-	108	-
		6	83	-	-	75	-	113	-
		9	75	-	-	85	-	105	-
		13	80	-	-	80	-	75	-
524		0	-	-	98	-	190	-	-
		2	-	-	88	-	165	-	-

Ride Quality

MnDOT's Lightweight Profiler, conforming to ASTM E-950 requirements (Figure 19) was used for collection of the ride quality data in terms of the International Roughness Index (IRI) according to the following timeline:

Reference Concrete (Cell 524): testing was performed on October 26th, 2017, as well as April 25th, June 11th, August 16th, and October 2nd 2018 on both the inside and outside traffic lanes

Low Cement Concrete (Cell 138): testing was performed on July 18th, July 20th, July 25th, November 3rd, and November 30th 2017, as well as June 14th, July 9th, and July 26th 2018 on both the inside and outside traffic lanes

Lower Cement Concrete (Cell 238): testing was performed on July 18th, July 20th, and July 25th, November 3rd, and November 30th 2017, as well as June 14th, July 9th, and July 26th 2018 on both the inside and outside traffic lanes

Figure 19- MnDOT's Lightweight Profiler

Tables 13-15 summarize the IRI data obtained for the investigated pavements. The reported data are the average of three IRI readings from both the right and left wheel tracks, along with the corresponding Mean Roughness Index (MRI) values. Figure 20 also presents the variation in MRI values over time, for both the inside and outside lanes of the investigated cells during the first year.

The data obtained for the reference cell (Cell 524) revealed consistent performance over time, with no significant difference between measurements performed in October 2017 and the ones taken in October 2018. The MRI values obtained for the outside lane of Cell 524 were constantly higher than those obtained for the inside lane which is exposed to controlled traffic loading. One should note the difference in thickness of the investigated pavements, where the reference cell is 6.0 in. thick, compared to 8.0-in. thick pavement at Cells 138 and 238.

Comparable performance was observed for the Cells 138 and 238 for the first year. The MRI values obtained for the outside lane were generally lower than the ones recorded for the inside lane (exposed to traffic) at Cell 138. The minimum MRI values were recorded during the first month from construction with values limited to 108 in./mile for both cells. However, an increase in MRI was observed for the measurements taken during the period of November 2017 to July 2018. The increase in MRI was more pronounced for the inside lane which can be due to the exposure to traffic loading. The MRI values obtained for the inside lane ranged from 106 to 139, and from 86 to 110 in./mile for Cells 138 and 238, respectively.

It should be noted that a MRI of no more than 65 in./mile is typically recommended by MNDOT. Given the short length of the test cells, such low IRI values are hard to achieve during paving. However, the presented data will only serve as the baseline for comparing the performance of the low cement pavement sections over time. Further data will be available for future annual cell performance reports.

Table 13- Ride quality data for Cell 524

Concrete Type	Test Date	Lane	Wheel path	IRI (in./mile)	MRI (in./mile)
Reference; Cell 524	10/26/2017	Inside	Left	93.2	99.1
			Right	105.0	
		Outside	Left	101.1	108.1
			Right	115.1	
	03/28/2018	Inside	Left	84.4	89.2
			Right	94.0	
		Outside	Left	93.2	101.2
			Right	109.2	
	04/25/2018	Inside	Left	81.1	85.0
			Right	88.8	
		Outside	Left	85.2	90.6
			Right	96.0	
	06/11/2018	Inside	Left	100.4	110.6
			Right	120.8	
		Outside	Left	109.7	115.9
			Right	122.1	
	08/16/2018	Inside	Left	85.0	89.1
			Right	93.3	
		Outside	Left	94.8	99.2
			Right	103.6	
	10/02/2018	Inside	Left	86.5	95.9
			Right	105.2	
		Outside	Left	96.3	102.3
			Right	108.3	

Table 14- Ride quality data for Cell 138

Concrete Type	Test Date	Lane	Wheel path	IRI (in./mile)	MRI (in./mile)
Low cement; Cell 138	07/18/2017	Inside	Left	112.7	108.1
			Right	103.5	
		Outside	Left	116.0	102.6
			Right	89.1	
	07/20/2017	Inside	Left	112.5	107.8
			Right	103.1	
		Outside	Left	115.7	102.2
			Right	88.6	
	07/25/2017	Inside	Left	114.5	106.9
			Right	99.2	
		Outside	Left	114.5	101.1
			Right	87.8	
	11/03/2017	Inside	Left	136.35	135.40
			Right	134.64	
		Outside	Left	86.11	88.70
			Right	91.49	
	11/30/2017	Inside	Left	134.13	137.49
			Right	140.98	
		Outside	Left	87.75	90.60
			Right	93.65	
	06/14/2018	Inside	Left	120.45	124.38
			Right	128.37	
		Outside	Left	157.77	139.39
			Right	121.52	
	07/09/2018	Inside	Left	116.84	106.89
			Right	96.75	
		Outside	Left	109.87	110.25
			Right	110.56	
	07/26/2018	Inside	Left	141.80	139.39
			Right	136.79	
		Outside	Left	107.97	100.93
			Right	93.96	

Table 15- Ride quality data for Cell 238

Concrete Type	Test Date	Lane	Wheel path	IRI (in./mile)	MRI (in./mile)
Lower cement; Cell 238	07/18/2017	Inside	Left	100.8	89.6
			Right	78.5	
		Outside	Left	97.7	104.3
			Right	111.0	
	07/20/2017	Inside	Left	100.8	89.7
			Right	78.6	
		Outside	Left	100.8	105.0
			Right	109.2	
	07/25/2017	Inside	Left	98.2	87.1
			Right	75.9	
		Outside	Left	100.8	104.5
			Right	108.2	
	11/03/2017	Inside	Left	93.52	86.80
			Right	80.09	
		Outside	Left	124.63	133.50
			Right	142.12	
	11/30/2017	Inside	Left	118.48	110.44
			Right	102.45	
		Outside	Left	125.01	132.61
			Right	140.47	
	06/14/2018	Inside	Left	116.77	110.25
			Right	103.66	
		Outside	Left	90.54	94.41
			Right	98.71	
	07/09/2018	Inside	Left	93.58	87.88
			Right	82.37	
		Outside	Left	114.30	115.13
			Right	115.57	
	07/26/2018	Inside	Left	104.42	94.85
			Right	85.22	
		Outside	Left	129.63	133.69
			Right	137.55	

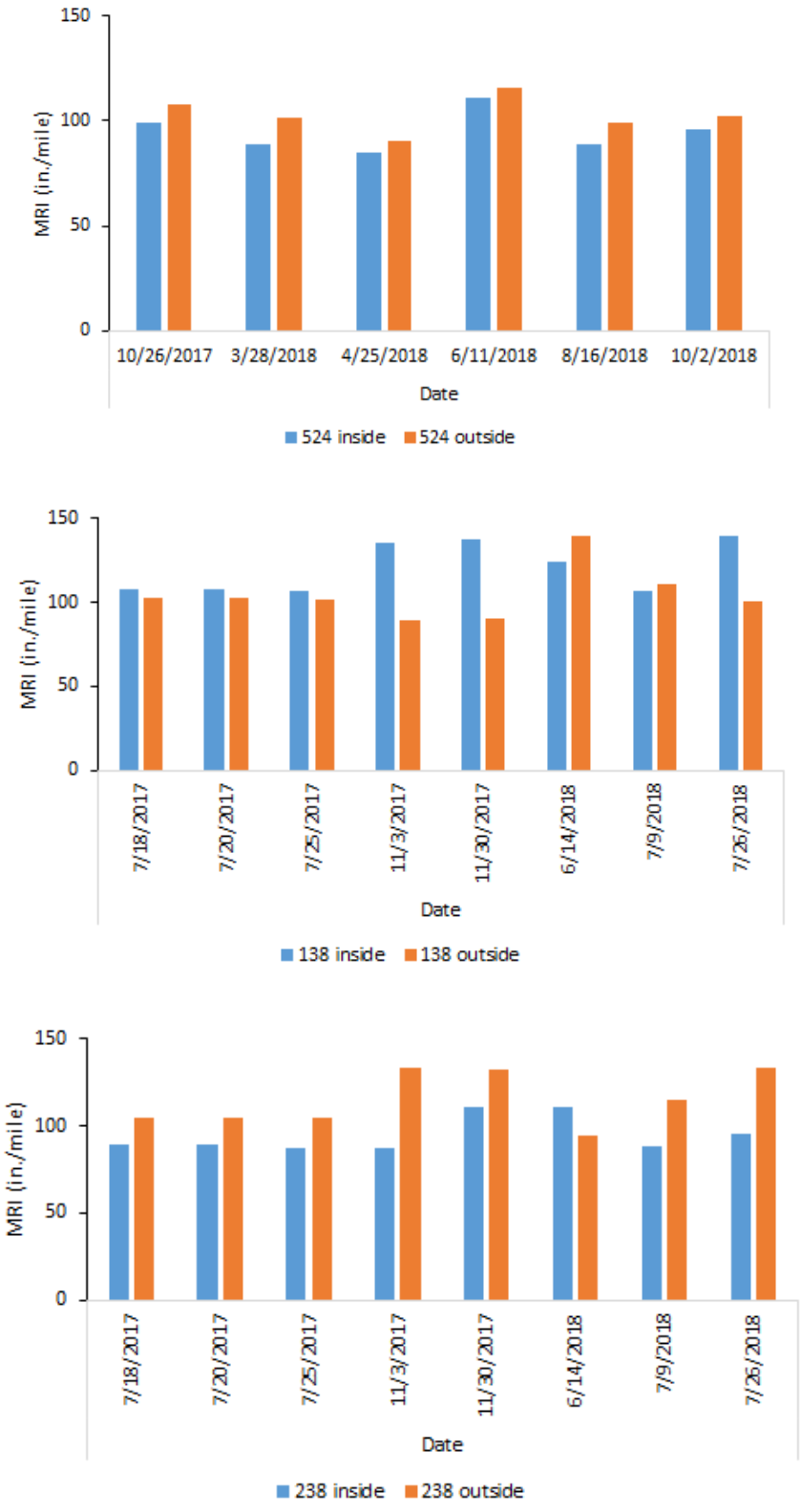

Figure 20- Variation in MRI (in./mile) values as a function of time

Dynamic Load Test

A 5-axle, 18-wheel semi-tractor trailer with total weight of 80 kips was used for loading the pavement sections. Figure 21 offers a schematic view of the vehicle configurations. Table 16 summarizes the axle loads. Testing was conducted on pavement cast with low and lower cement content on September 9th, 2017, March 21st, 2018, and May 2nd, 2018. The loading was conducted at two speed levels of 5 and 35 mph, replicated five times per speed scenario. For each pavement type, response to the dynamic lading was recorded by 8 sensors, installed at different depths and locations as detailed in Figure 22. The CE sensors measure the dynamic strain gages and VWs are the vibrating wire strain gages. The investigated sensors were located at top and bottom of the slabs, at both the corner and mid-edge spots of the instrumented panels, as detailed in Table 17 and Table 18.

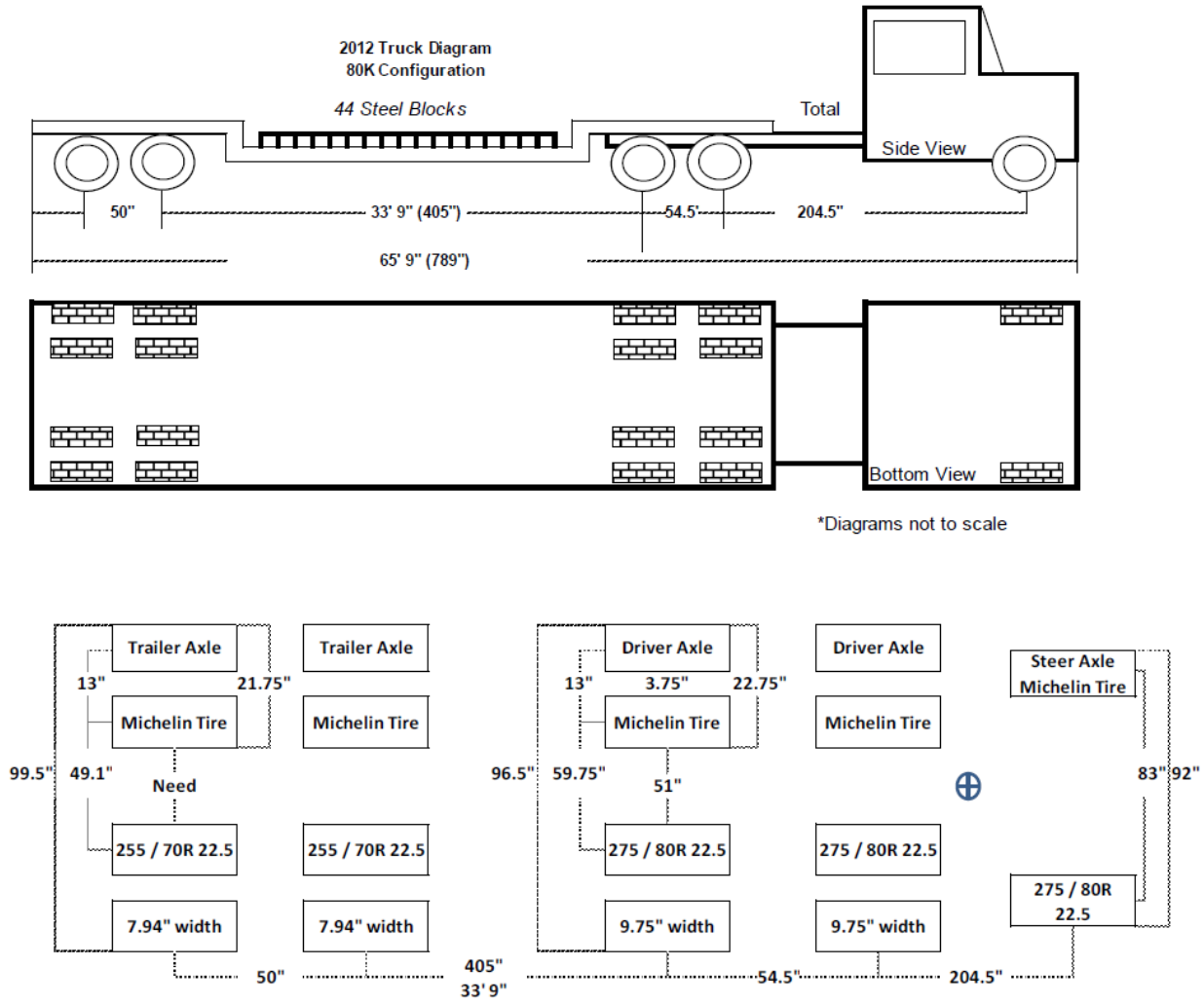

Figure 21- Vehicle dimensions and axle configurations for the Workstar truck and the Towmaster trailer employed for dynamic loading (MnDOT 2013)

Table 16- Axle weight for the Workstar truck and the Towmaster trailer employed for dynamic loading (MnDOT 2013)

	Tractor	Tractor Tandem		Trailer Tandem	
Total Weight	Steering Axle	Front Axle	Back Axle	Front Axle	Back Axle
79,700	11,700	17,650	16,450	16,800	17,100
		34,100		33,900	

Figure 22- Sensor installation plan for Cell 138 (top) and Cell 238 (bottom).

Table 17- As-built location of sensors installed in mixtures prepared with low and lower cementitious materials content

Cell 138				Cell 238			
Sensor #	**Station**	**Offset (ft)**	**Depth (in.)**	**Sensor #**	**Station**	**Offset (ft)**	**Depth (in.)**
CE001	9353.95	11.2	0.8	CE001	9474.07	10.9	0.8
CE002	9353.95	11.2	7.5	CE002	9474.07	10.9	7.5
CE003	9360.01	11.0	0.8	CE003	9480.08	10.9	0.8
CE004	9360.01	11.0	7.5	CE004	9480.08	10.9	7.5
CE005	9368.98	10.8	0.8	CE005	9489.07	10.9	0.8
CE006	9368.98	10.8	7.5	CE006	9489.07	10.9	7.5
CE007	9374.97	10.8	0.8	CE007	9495.02	11.1	0.8
CE008	9374.97	10.8	7.5	CE008	9495.02	11.1	7.5
VW001	9384.13	11.0	0.8	VW001	9459.00	10.9	0.8
VW002	9384.13	11.0	7.5	VW002	9459.00	10.9	7.5
VW003	9390.16	6.0	0.8	VW003	9464.98	6.0	0.8
VW004	9390.16	6.0	7.5	VW004	9464.98	6.0	7.5

Table 18- Detailed layout of the sensors embedded in Cell 138 and Cell 238

Cell 138 & 238			
Location in Slab	**Depth**	**Orientation**	**Sensor #**
Corner	Top	Transverse	CE001
		Transverse	CE005
	Bot.	Transverse	CE002
		Transverse	CE006
Mid-Edge	Top	Longitudinal	CE003
		Longitudinal	CE007
	Bot.	Longitudinal	CE004
		Longitudinal	CE008

Data was recorded with a frequency of 1200 Hz. The total test time was about 5 and 20 s for loading at 35 and 5 mph, respectively. The average of readings obtained through first 2 and 0.5 seconds were calculated and employed as the base line for normalizing the data for 5 and 35 mph scenarios, respectively. Figure 23 presents an example of traffic loading data obtained from Sensor # CE008, located at bottom part, mid-edge of Cell 238. Given the high frequency of data recording, trend lines were developed for further clarification of the load-deflection patterns as shown in Figure 23. Note that the scattered blue lines are the normalized raw data and the trend line is shown in yellow, which clearly depicts the local maxima under the front wheel and the rear tandem axels.

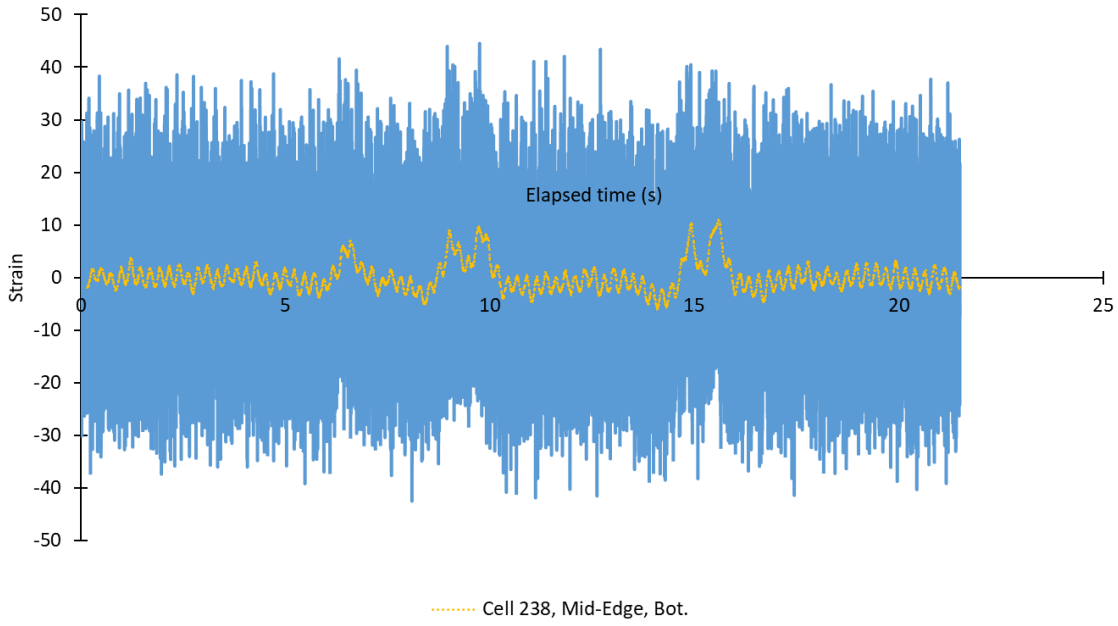

Figure 23- Sample raw data and corresponding trend line obtained from dynamic load test

Figure 24 and Figure 25 present the trend lines observed for sensors embedded at different depths and different spots of pavements made with low and lower cementitious materials content. Change in direction of stress was observed with the load moving on the pavement surfaces. Trends were similar for the data obtained from both cells cast with Low or Lower cementitious materials content. Results indicate similar performance for the two sensors located at the same depth and the same spot of the panels within the same concrete type. Comparable responses were obtained for loading the pavement at 5 and 35 mph, for a given combination of test spot, sensor depth, and concrete type. However, deformations were higher for the sensors located at mid-edge compared to those located at corner of the slabs. Moreover, the sensors embedded at bottom and top of the mid-edge spots exhibited more symmetrical data, corresponding to compressive and tensile strains (and stresses) induced by the moving truck.

In general data obtained during the dynamic load testing suggest similar performance of the investigated cells. This could be expected, given the comparable mechanical properties, same thickness, and similar subgrade conditions of the two test cells. The presented data will act as a baseline for future measurements to highlight the potential variations in load-deflection performance of the pavements over time.

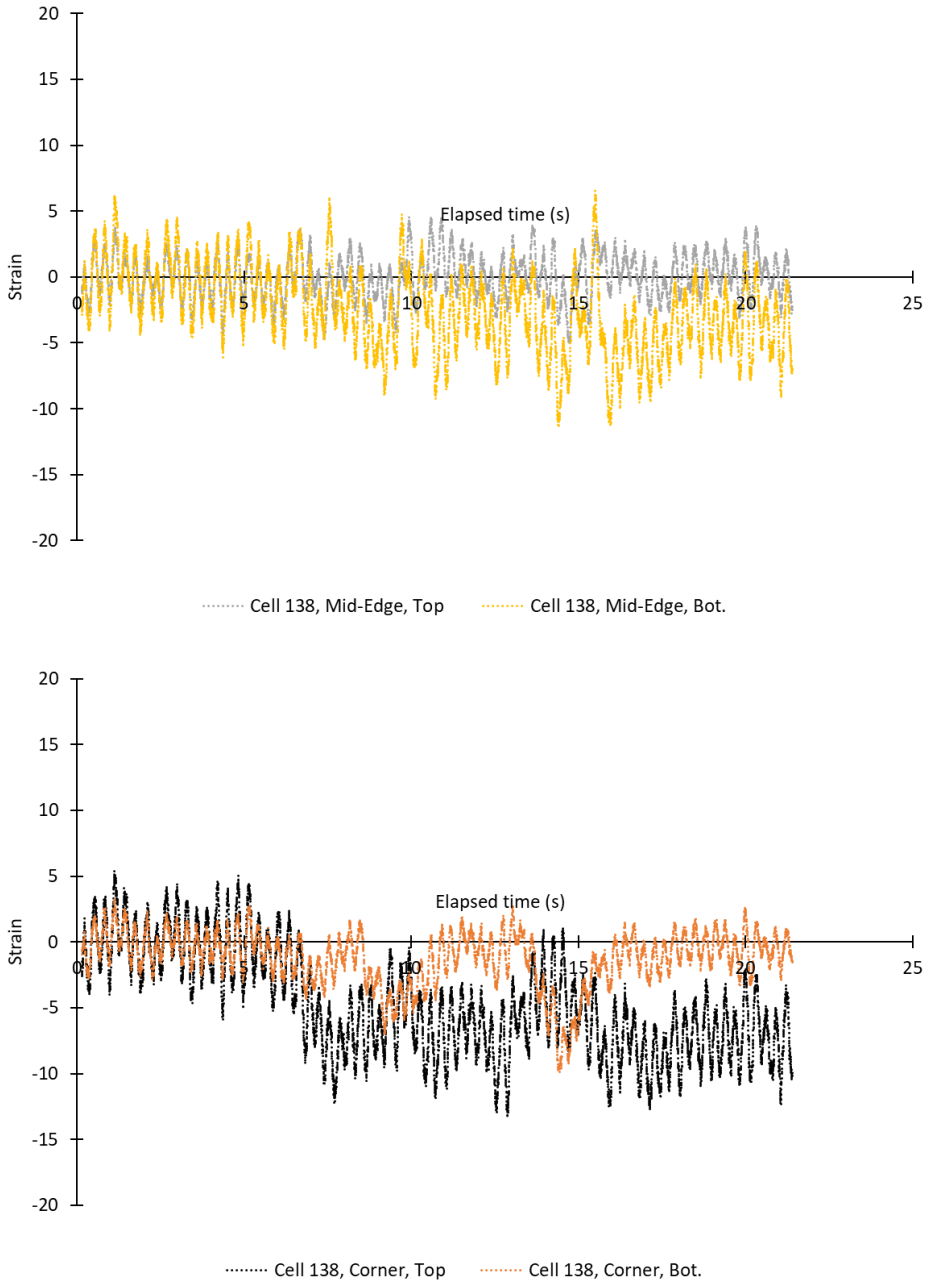

Figure 24- Load-deflection patterns for Cell 138 at corner and mid-edge

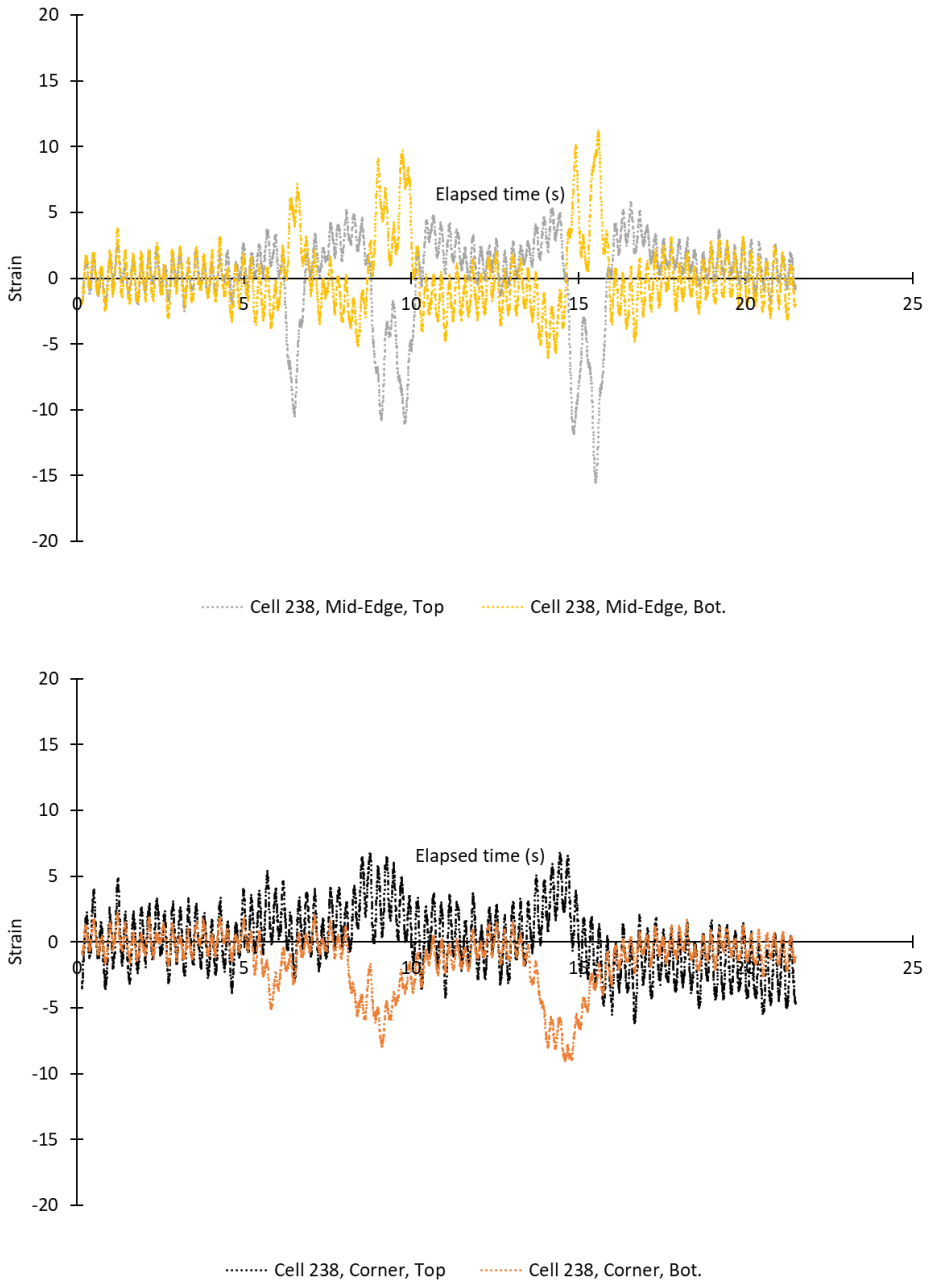

Figure 25- Load-deflection patterns for Cell 238 at corner and mid-edge

Table 19 summarizes the minimum and maximum strain values obtained for sensors located at top and bottom parts of the investigated panels. It should be noted that even though the loading test was performed five times for each section, the first sets of measurements yielded significantly lower strain values in all test scenarios. Therefore, the presented data are the average values for four measurements conducted at 5 and 35 mph. Moreover, the reported values were not corrected for traffic wander.

The values reported in this table are high for an 8.0 in. thick pavement. But this can be in part due to the noise in recording the data. The maximum and minimum strain values were comparable for both concrete types and did not follow a constant pattern favoring a certain mixture. In other words, the variation in cementitious materials content did not have a significant effect on registered maximum and minimum values and the investigated cells exhibited comparable response to traffic loading. This was in line with the comparable load-deflection patterns obtained for the mixtures presented in Figure 24 and Figure 25.

Table 19- Summary of the Max. and Min. strain values obtained through different testing scenarios for sensors embedded in Cell 138 and Cell 238

Cell #				**138**				**238**			
Location on Slab				**Corner**		**Mid-Edge**		**Corner**		**Mid-Edge**	
Depth				**Top**	**Bot.**	**Top**	**Bot.**	**Top**	**Bot.**	**Top**	**Bot.**
5 mph	09/13/2017	Avg.	Min.	-104	-59	-110	-60	-117	-54	-133	-55
			Max.	46	37	41	49	43	27	34	42
		Std.	Min.	7	6	8	8	17	5	4	10
			Max.	3	3	2	4	3	1	1	1
	03/21/2018	Avg.	Min.	-157	-62	-170	-70	-92	-42	-92	-50
			Max.	61	54	50	66	52	32	37	49
		Std.	Min.	4	8	7	8	29	6	31	6
			Max.	1	1	1	4	1	1	3	4
	05/02/2018	Avg.	Min.	-121	-55	-126	-57	-137	-53	-151	-56
			Max.	32	28	31	36	69	35	42	62
		Std.	Min.	17	7	16	6	12	3	11	1
			Max.	1	0	2	1	4	2	4	7
35 mph	09/13/2017	Avg.	Min.	-104	-56	-109	-61	-129	-59	-132	-67
			Max.	40	33	35	40	35	22	28	33
		Std.	Min.	14	8	11	12	7	6	4	4
			Max.	3	2	3	2	3	2	2	1
	03/21/2018	Avg.	Min.	-155	-65	-168	-76	-102	-52	-109	-54
			Max.	57	51	48	62	50	29	32	42
		Std.	Min.	22	15	19	14	18	11	9	12
			Max.	4	4	2	3	12	2	2	6
	05/02/2018	Avg.	Min.	-142	-73	-149	-84	-152	-58	-159	-67
			Max.	69	52	54	76	61	32	37	51
		Std.	Min.	12	6	9	6	20	13	16	18
			Max.	5	5	1	6	6	2	2	4

In-Situ Static Deformation

Vibrating wire strain gages (VWSG) embedded at corner and mid-panel areas were used to monitor the total in-situ deformations due to environmental loads. The recorded deformations were caused by a combination of concrete shrinkage, warping due to moisture loss, curling due to temperature gradient within the depth of concrete, and linear deformation of the sensors and the surrounding concrete due to variations in temperature. Figure 26 presents the strain history recorded during the first year from casting the cells. Time zero readings correspond to the strain values at the time of placing the concrete. For both mixtures, VWSG 1 and VWSG 3 present the deformations close to the surface of the concrete, at corner and mid-panel, respectively, while VWSG 2 and VWSG 4 present the deformations at bottom part of the concrete, at corner and mid-panel, respectively. VWSG 1 and VWSG 2 had transverse orientation, while VWSG 3 and VWSG 4 were oriented longitudinally.

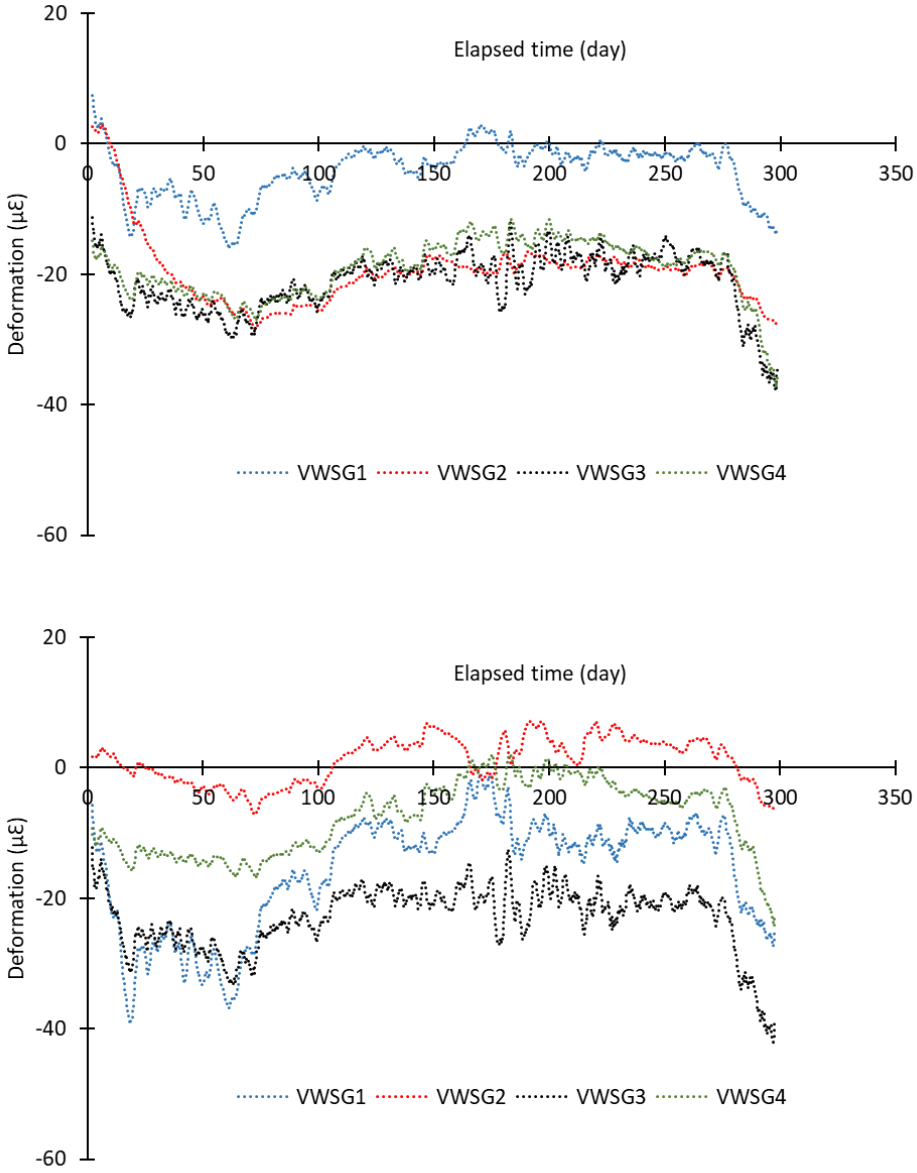

Figure 26- Total in-situ deformation (με) for Cell 138 (top) and 238 (bot.)

In general, the investigated sensors exhibited similar deformation pattern, with a tendency towards negative strain values, corresponding to compressive stresses during the first 75 days, i.e. late August 2017. This was followed by a change in patterns, switching towards positive strain values, i.e. tensile stresses. The changes in direction of recorded strain and stresses after about 75 days can be due to the seasonal variations in ambient temperature, where a drop in temperature can be noticed as shown in Figure 27, and relative humidity with the start of cold season. The sensors located at top parts of the pavement exhibited slightly higher sensitivity to such seasonal effects, with a wider range of variation between the recorded minimum and maximum strain values. This was more pronounced for the pavement cast with lower cementitious content.

The total in-situ deformations were limited to 40 με, regardless of the concrete type and sensor depth and location, indicating similar response of the investigated cells to environmental conditions. Such a similar response to environmental effects is in line with the previous observations, including the comparable MOE, CTE, and shrinkage values, similar thickness and subgrade conditions, and similar exposure conditions. The research team will monitor the performance of the pavements for the next two years and compare the deformation patterns over the following cold/hot seasons.

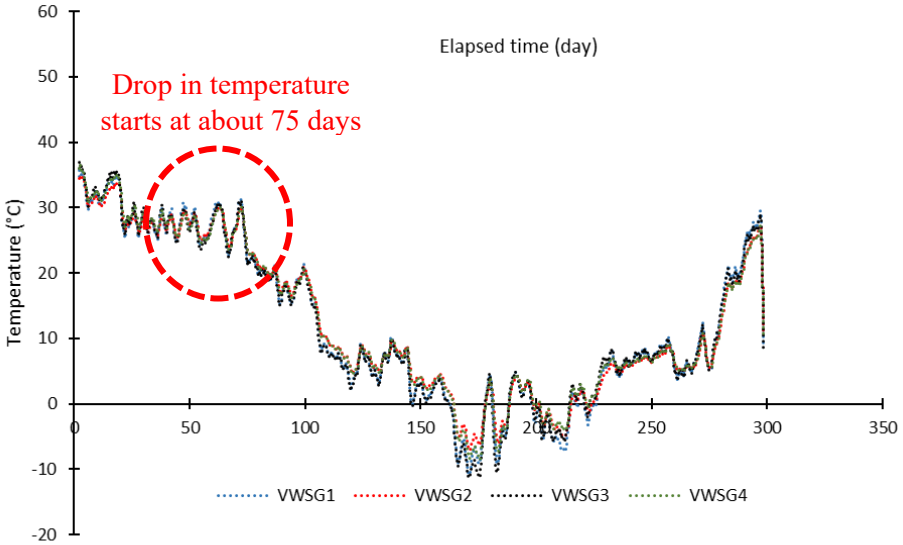

Figure 27- Variation in concrete temperature registered by the VWSGs embedded at Cell 238

Evaluating Joint Activation using MIRA test

On September 21st, 2017, a non-destructive test method based on ultrasonic shear-wave tomography was employed to explore the joint activation. The MIRA device (Figure 28) contains 40 dry point contact (DPC) transducers that send and receive low-frequency (55 kHz) shear-wave ultrasonic pulses (Vosoughi and Taylor 2017). The test was repeated 10 times at each joint, and the average results were reported. Figure 29 presents sample processed data obtained from MIRA test. The left figure is the filter signal and the right figures are obtained by normalizing the transmitted energy across each transducer to transmitted energy of transducer number 6 for determining whether or not cracking occurred at the joint. Normalized values lower than the threshold suggest crack development at examined joints.

Figure 28- Mira test setup

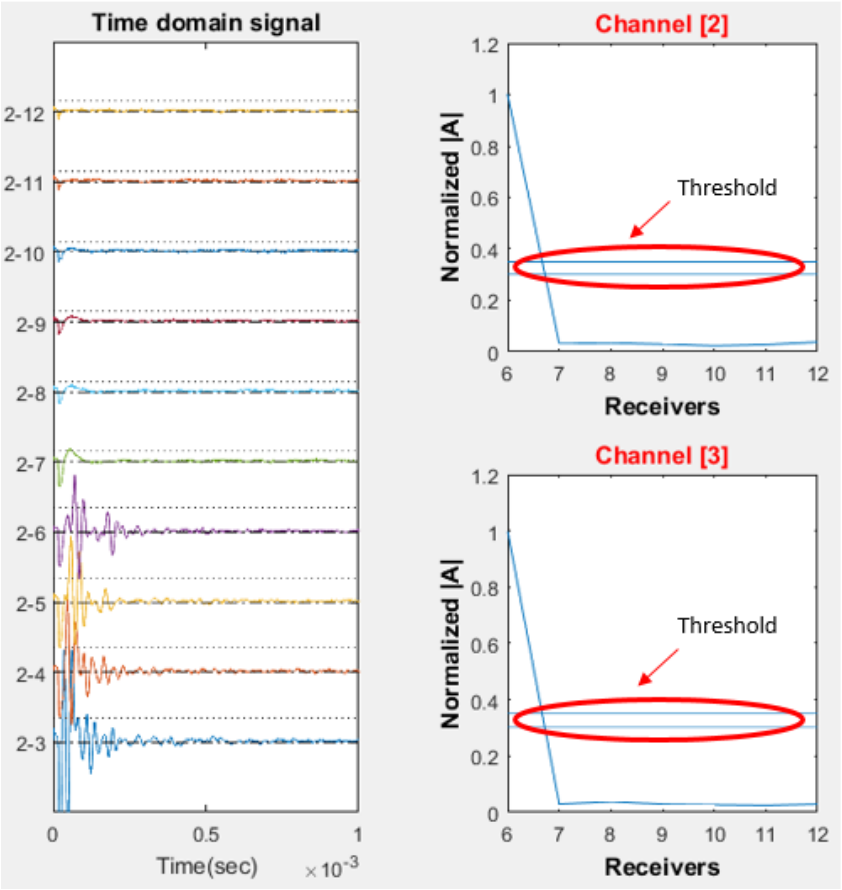

Figure 29- Processed Mira test data

Figure 30 summarizes the MIRA test results. The obtained data indicated cracking in all joints within Cells 138 and 238. No cracking was observed at the joints at the ends of the section, i.e. joints A and C

shown in Figure 30. The outside lane only experiences the environmental loads, while the inside lane is loaded by MnROAD 80k truck.

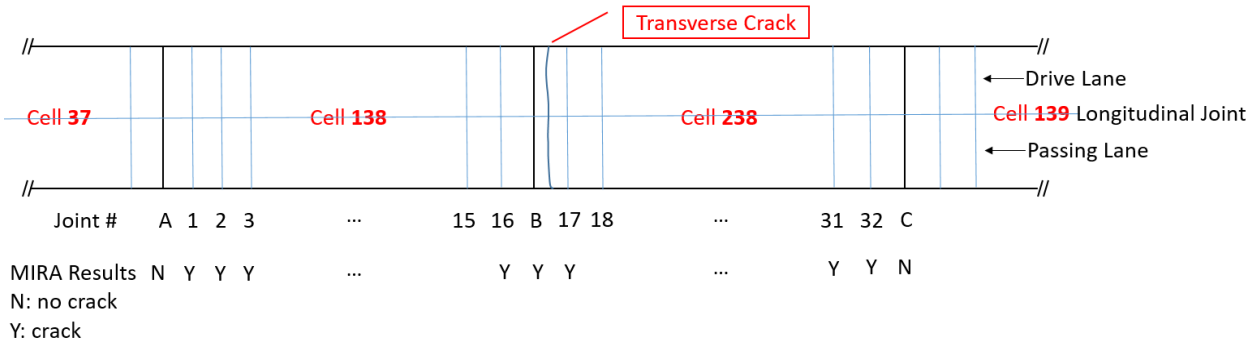

Figure 30- Joint cracking map – All joints deployed by the measurement event on 09/21/2017

Distress Survey

It was reported by MnDOT staff that a transverse crack was observed on February 27, 2018, on the first panel transition from Cell 138 to 238 across both inside and outside lanes. The crack is about 5 feet from the downstream joint and angling slightly away from mid-panel as shown in Figure 31. The cause of the crack is still under investigation.

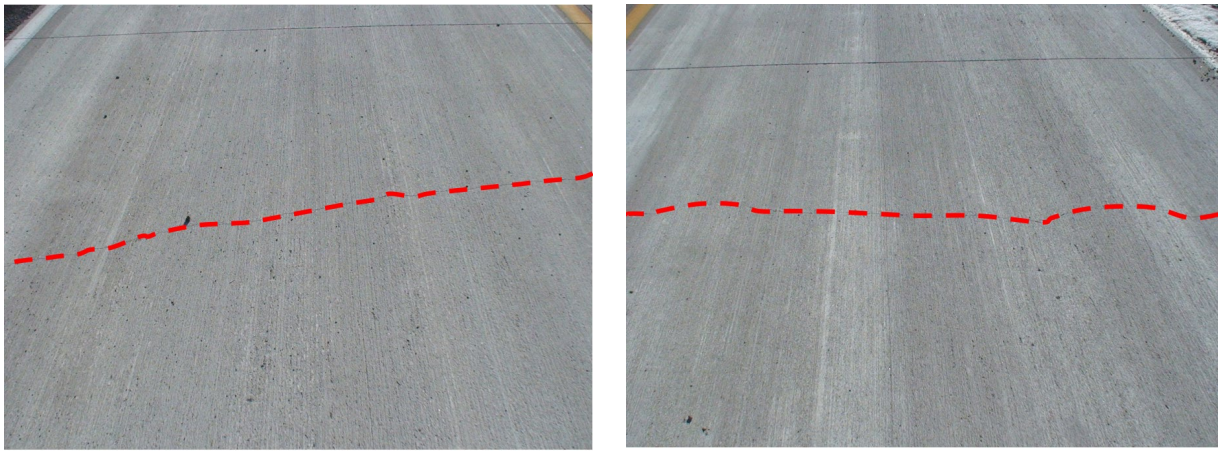

Figure 31- Transverse crack occurred on outside lane (left) and inside lane (right) at Cell 238

Further cracking (Figure 32) was observed in July 2018 near the wheel path at Cell 238, cast with concrete with lower cementitious materials content. The distress will be investigated by the research team to elucidate the reason for such distress and results will be discussed in the upcoming performance reports.

Figure 32- Further distress in form of cracking near the wheel path at Cell 238

KEY FINDINGS

Based on the presented results, the following findings are developed:

- The mixture prepared with low cementitious materials content of 500 lb/yd^{3}exhibited acceptable workability based on VKelly and Box test results. Slight workability problems were observed for the mixture with lower cementitious materials content of 470 lb/yd^3.
- Both mixtures exhibited acceptable 28-day compressive strength of over 3,500 psi as specified in AASHTO PP 84. Both mixtures developed compressive strength of 3,000 psi before 14 days, which is MnDOT's strength requirement for opening to traffic.
- The hardened air void data indicated an acceptable air void system for both concrete types. Moreover, the investigated mixtures developed adequate surface resistivity corresponding to "Very Low" risk of chloride ion penetration at 91 days.
- Measurements on potential for oxychloride formation indicate some risk of damage due to de-icing salts for both concrete mixtures.
- MIRA measurements indicated cracking in all joints along the experimental section regardless of the cementitious materials content.
- The pavement cast with low and lower cementitious materials exhibited comparable LTE with average values ranging from 80% to 97%, while lower LTE was observed for the reference concrete with average values of 85±1%. The LTE was slightly higher for the departure traffic, i.e. test after joint.
- Both pavements cast with low or lower cementitious content had similar response to the controlled traffic loading, in terms of the general deformation pattern and the recorded maximum and minimum values. Sensors embedded at same depth and spot in the slabs exhibited similar deformation patterns.
- The long-term in-situ deformations were limited to 40 με for both mixtures, where variation in direction of stresses and strains were dominated by the environmental effects regardless of the concrete mixture type.
- In general, and based on the first year performance data, it was concluded that both cells cast with low and lower cementitious materials exhibit comparable performance in terms of material properties and in-situ response to environmental conditions and traffic loading.

REFERENCES

American Association of State Highway and Transportation Officials (AASHTO). 2017. *Developing Performance Engineered Concrete Pavement Mixtures*. AASHTO PP 84. AASHTO, Washington, DC.

American Association of State Highway and Transportation Officials (AASHTO). 2011. *Standard Method of Test for Surface Resistivity Indication of Concrete's Ability to Resist Chloride Ion Penetration*. AASHTO TP 95. AASHTO, Washington, DC.

American Association of State Highway and Transportation Officials (AASHTO). 2017. *Standard Method of Vibrating Kelly Ball (VKelly) Penetration in Fresh Portland Cement Concrete*. AASHTO TP 129. AASHTO, Washington, DC.

American Association of State Highway and Transportation Officials (AASHTO). 2015. *Coefficient of Thermal Expansion of Hydraulic Cement Concrete*. AASHTO T 336. AASHTO, Washington, DC.

ASTM C29 / C29M-17a, *Standard Test Method for Bulk Density ("Unit Weight") and Voids in Aggregate*, ASTM International, West Conshohocken, PA, 2017

ASTM C39 / C39M-18, *Standard Test Method for Compressive Strength of Cylindrical Concrete Specimens*, ASTM International, West Conshohocken, PA, 2018

ASTM C150 / C150M-17, Standard Specification for Portland Cement, ASTM International, West Conshohocken, PA, 2017

ASTM C157 / C157M-17, Standard Test Method for length Change of Hardened Hydraulic-Cement Mortar and Concrete, ASTM International, West Conshohocken, PA, 2017

ASTM C231 / C231M-17a, *Standard Test Method for Air Content of Freshly Mixed Concrete by the Pressure Method*, ASTM International, West Conshohocken, PA, 2017

ASTM C457 / C457M-16, *Standard Test Method for Microscopical Determination of Parameters of the Air-Void System in Hardened Concrete*, ASTM International, West Conshohocken, PA, 2016

ASTM C469 / C469M-14, *Standard Test Method for Static Modulus of Elasticity and Poisson's Ratio of Concrete in Compression*, ASTM International, West Conshohocken, PA, 2014

ASTM C618-17a, *Standard Specification for Coal Fly Ash and Raw or Calcined Natural Pozzolan for Use in Concrete*, ASTM International, West Conshohocken, PA, 2017

ASTM C1753 / C1753M-15e1, *Standard Practice for Evaluating Early Hydration of Hydraulic Cementitious Mixtures Using Thermal Measurements*, ASTM International, West Conshohocken, PA, 2015

ASTM E2583-07(2015), *Standard Test Method for Measuring Deflections with a Light Weight Deflectometer (LWD)*, ASTM International, West Conshohocken, PA, 2015

ASTM E950-98, *Standard Test Method for Measuring the Longitudinal Profile of Traveled Surfaces with an Accelerometer Established Inertial Profiling Reference*, ASTM International, West Conshohocken, PA, 1998

Cook, D., Ghaeezadah, A., and Ley, T. 2014. *A Workability Test for Slip Formed Concrete Pavements*. Construction and Building Materials, Vol. 68, pp. 376–383.

Kennedy, T., Huber, G., Harrigan, E., Cominsky, R., Hughes, C., Quintus, H., and Moulthrop. J. 1994. *Superior Performing Asphalt Pavements (Superpave): The Product of SHRP Asphalt Research Program*. Strategic Highway Research Program, Washington, DC.

Ley, T. 2013. *Super Air Meter*, Tech Brief, National Concrete Pavement Technology Center, Ames, IA.

Ley, T., Cook, D., and Fick. G. 2012. *Concrete Pavement Mixture Design and Analysis (MDA): Effect of Aggregate Systems on Concrete Properties*, National Concrete Pavement Technology Center, Ames, IA.

Minnesota Department of Transportation (MnDOT). 2013. *MnROAD Semi Tractor Trailrer*. MnDOT, St. Paul, MN.

http://www.dot.state.mn.us/mnroad/data/pdfs/semidescription.pdf

Minnesota Department of Transportation (MnDOT). 2016. *Standard Specifications for Construction. Section 2301: Concrete Pavement*. MnDOT, St. Paul, MN. https://www.dot.state.mn.us/materials/concretedocs/Section_3_2301_Specifications.pdf

Monical, J., Villani, C., Farnam, Y., Unal, E., and Weiss W. J. 2016. *Using Low-Temperature Differential Scanning Calorimetry to Quantify Calcium Oxychloride Formation for Cementitious Materials in the Presence of Calcium Chloride*. Advances in Civil Engineering Materials, Vol. 5, No. 1.

Shilstone, J. M. 1990. *Concrete Mixture Optimization*. Concrete International, American Concrete Institute (ACI), 12(6): 33–39.

Taylor, P., Wang, X., and Wang, X. 2015. *Concrete Pavement Mixture Design and Analysis (MDA): Development and Evaluation of Vibrating Kelly Ball Test (VKelly Test) for the Workability of Concrete*. National Concrete Pavement Technology Center, Ames, IA.

Vosoughi, P., Taylor, P., *Impacts of Internal Curing on the Performance of Concrete Materials in the Laboratory and the Field*. National Concrete Pavement Technology Center, Ames, IA.